INTEGRATION AND SEGREGATION PROCESSES IN MOTION PERCEPTION

by
M. İLKER DUYMAZ

Submitted to the Graduate School of Social Sciences
in partial fulfilment of
the requirements for the degree of Master of Science

Sabancı University
July 2023

INTEGRATION AND SEGREGATION PROCESSES IN MOTION PERCEPTION

Approved by:

Asst. Prof. NİHAN ALP .....
(Thesis Supervisor)

Assoc. Prof. İNCİ AYHAN .....

Asst. Prof. EREN GÜNSELİ .....

Date of Approval: July 17, 2023

ABSTRACT

INTEGRATION AND SEGREGATION PROCESSES IN MOTION PERCEPTION

M. İLKER DUYMAZ

PSYCHOLOGY M.S. THESIS, JULY 2023

Thesis Supervisor: Asst. Prof. NİHAN ALP

Keywords: motion perception, motion integration, steady-state visually evoked potentials

The perception of motion requires the visual system to integrate inputs from various stages of motion processing. This thesis aims to contribute to our understanding of motion integration. Two studies were conducted for this purpose. The first study investigates how different motion perception systems integrate visual features. Our findings reveal that the position-based motion system, a motion perception system that relies on attentive tracking of object positions, binds moving features based on static cues like proximity and similarity. In contrast, the velocity-based motion system, which utilizes direction-selective cells, largely disregards these static cues. These results support previous findings that these motion systems can extract different motion information from the same stimulus. Furthermore, the discovery of distinct integration rules between these systems provides a novel contribution to the existing knowledge on motion integration. The second study addresses a limitation of the SSVEP methodology in motion perception research. It reveals that large-scale cortical dynamics can generate SSVEPs that mimic those produced by motion-sensitive neural populations by interacting with moving stimuli. We propose that randomizing the phase of position modulations across trials can overcome this issue by eliminating SSVEPs generated by large-scale cortical dynamics. These technical advancements have implications for past and future motion integration studies utilizing SSVEPs.

ÖZET

HAREKET ALGISINDAKİ ENTEGRASYON VE SEGREGASYON SÜREÇLERİ

M. İLKER DUYMAZ

PSİKOLOJİ YÜKSEK LİSANS TEZİ, TEMMUZ 2023

Tez Danışmanı: Dr. Öğr. Üyesi NİHAN ALP

Anahtar Kelimeler: hareket algısı, hareket algısında entegrasyon, frekans etiketleme

Beyinde görsel hareket algısını sağlayan işlemler görsel bilginin farklı aşamalarda entegre edilmesini gerektirir. Bu tez, görsel hareketin beyinde nasıl entegre edildiğiyle ilgili mevcut bilgiyi artırmayı hedefleyen iki çalışmadan oluşmaktadır. İlk çalışma beyindeki farklı hareket algılama sistemlerinin hareket eden görsel unsurları nasıl birleştirdiği hakkındadır. Bu çalışmadaki bulgularımız, hareket algısını sağlayan iki farklı sistemin görsel unsurları farklı kurallara göre gruplandırdığına işaret etmektedir. Nesnelerin pozisyonlarının zamansal değişimlerini takip ederek hareket algısını sağlayan pozisyon bazlı hareket algısı sisteminin görsel unsurları benzerlik ve yakınlık gibi durağan özelliklere göre gruplandırdığı gözlemlenmiştir. Diğer yandan, hareket yönüne duyarlı nöronlar yoluyla hareket algısını sağlayan velosite bazlı hareket algılama sisteminin bu durağan özellikleri dikkate almadığı gözlemlenmiştir. Bu sistemlerin görsel unsurları farklı kurallara göre birleştirdiği bulgusu literatüre özgün bir katkı sunmaktadır. İkinci çalışma EEG bazlı frekans etiketleme yönteminin hareket algısı çalışmalarında ortaya çıkabilecek bir limitasyonunu ele almaktadır. Bu çalışmada, beynin yapısal organizasyonunun hareket eden görsel unsurlarla etkileşimi sonucunda normal şartlar altında hareket bilgisini işleyen nöral popülasyonların aktivitesine atfedilebilecek fakat bu popülasyonların aktivitesinden bağımsız da ortaya çıkabilen yanıltıcı sonuçlar doğurabileceği bulunmuştur. Bu sorunu gidermek için hareket eden görsel unsurların pozisyon değişimlerinin fazını rastgeleleştirmek üzerine kurulu bir çözüm sunulmuştur.

ACKNOWLEDGEMENTS

I would like to express my deepest gratitude to my advisor, Dr. Nihan Alp. She believed in me more than I believed in myself, and continuously pushed me to reach new heights. Through her guidance, I accomplished feats that I would not have dared to undertake on my own. She allowed me to freely explore my scientific curiosities, leading to numerous experiments that, although not all included in this thesis, played a crucial role in shaping the questions addressed in this work, and contributed to my growth as a researcher. Her enthusiasm and willingness to tackle challenges constantly fueled my motivation, and she provided unwavering support during times when I struggled to maintain focus. I am sincerely grateful for her mentorship, and I truly hope that I have made her proud through my work.

I would also like to extend my heartfelt appreciation to my previous advisors, Drs. Jaap Munneke and Jennifer Corbett. I had the incredible fortune of crossing paths with them when I was a clueless undergraduate student, eager to delve into research but uncertain of where to begin. Their kindness, acceptance, willingness to impart knowledge, and patience with a curious yet troublesome student like myself were invaluable. It was through their guidance that I discovered my passion for science—an endeavor I intend to pursue throughout my life. The invaluable knowledge and skills I acquired in their laboratory have laid a solid foundation for my pursuit of a master's degree and, undoubtedly, beyond. I will forever be grateful to them for guiding me on my academic as well as personal journey.

I would also like to express my sincere gratitude to my dear friend Forrest Watson and his family. Forrest has been an incredible source of friendship and compassion, who has not only enriched my life but also profoundly shaped my perspective on the world, people, and life. His family has shown me unparalleled warmth and generosity, embracing me as one of their own. Their unwavering love and support have been invaluable during some of the most challenging periods of my life. It is through their spiritual guidance and encouragement that I found the strength to embark on my journey toward pursuing a master's degree. In recognition of their profound impact on my personal and academic growth, I dedicate this thesis to their lovely children, with whom I have shared countless joyful moments that have played a vital role in my healing process.

Last but certainly not least, I extend my sincere appreciation to my friends here at Sabancı University, particularly Ebru Ecem Tavacıoğlu, Xiermaimaiti Xiahamuhamaiti, Ecem Akın, and Cansu Kazan, for their invaluable support during data collection and for making this journey an enjoyable experience through their friendship.

To Davut, Aslan,
Nehir, and Cesur

TABLE OF CONTENTS

LIST OF FIGURES

LIST OF ABBREVIATONS

CCW Counter-clockwise 26, 29, 31, 32, 35

CW Clockwise 26, 29, 31, 32, 35

EEG Electroencephalography 3, 18, 20, 21, 22, 26, 27, 29, 38, 39, 40

FFT Fast Fourier Transform 28

IM Intermodulation 18, 19, 20

ISI Inter-stimulus interval 5, 9, 10, 11, 12, 13, 14, 15, 17, 19

PL Phase-locked 24, 25, 26, 27, 28, 29, 31, 32, 33, 34, 35, 36

PV Phase-varied 25, 26, 27, 28, 29, 31, 32, 33, 36

rm-ANOVA Repeated-measures analysis of variance 12, 29, 31, 32

ROI Region of interest 28, 29, 31, 32, 36

SNR Signal-to-noise ratio 29, 36

SSVEP Steady-state visually evoked potentials 3, 18, 20, 23, 32, 33, 41, 42, 43, 44

1. GENERAL INTRODUCTION

Integration is at the heart of visual perception. The entirety of the mechanisms that allow us to perceive the visual world around us depends on the hierarchical processing of information extracted by the photoreceptors in the retina. Individually, these photoreceptors have limited capabilities, solely capable of detecting light within very small regions of the retina. Yet, as the inputs from these photoreceptors progress to higher stages in the hierarchy of visual processing, they are integrated into increasingly specialized representations that cover larger areas of the visual field. Through this integration process, individual fragments of information are seamlessly combined, leading to a unified and detailed sensory experience.

As one of the hallmarks of visual perception, motion perception also relies primarily on the integration of visual information. In their seminal body of work, Hubel & Wiesel established the direction-selective cells as the primary units responsible for processing motion in the visual cortex (Hubel and Wiesel 1959, 1968). This discovery sparked extensive interdisciplinary investigations spanning several decades, aimed at understanding how the diverse range of motion phenomena could be computed through the integration of information derived from these cells (Adelson and Bergen 1985; Emerson, Bergen, and Adelson 1992; Reichardt 1961; Watson and Ahumada 1985). However, unraveling the intricate mechanisms underlying the integration of motion information in the visual system has proven to be a formidable challenge, given its multifaceted nature with numerous layers to explore.

The initial layer of complexity in motion integration arises from the inherent ambiguity of motion information extracted by individual direction-selective cells (Adelson and Movshon 1982; Marr and Ullman 1981; Wallach 1935). Due to their limited spatial extent, these cells can only detect local, unidirectional motion within their receptive field (Hubel and Wiesel 1959, 1968). However, these local motion cues can be compatible with multiple global motion directions (Figure 1.1). Known as the aperture problem, this inherent limitation of direction-selective cells results in ambiguity regarding the global motion direction based on their individual activity

(Adelson and Movshon 1982; Marr and Ullman 1981; Wallach 1935). Consequently, the visual system must first disambiguate the information from individual direction-selective cells to extract the global motion direction. Previously proposed solutions to the aperture problem primarily suggest that an integration of direction-selective cells takes place in early stages of motion processing to disambiguate motion direction (for a comprehensive review, see Nishida et al. 2018). Through this integration, the visual system generates a flow map of local motion vectors (Nishida et al. 2018).

Figure 1.1 Aperture problem

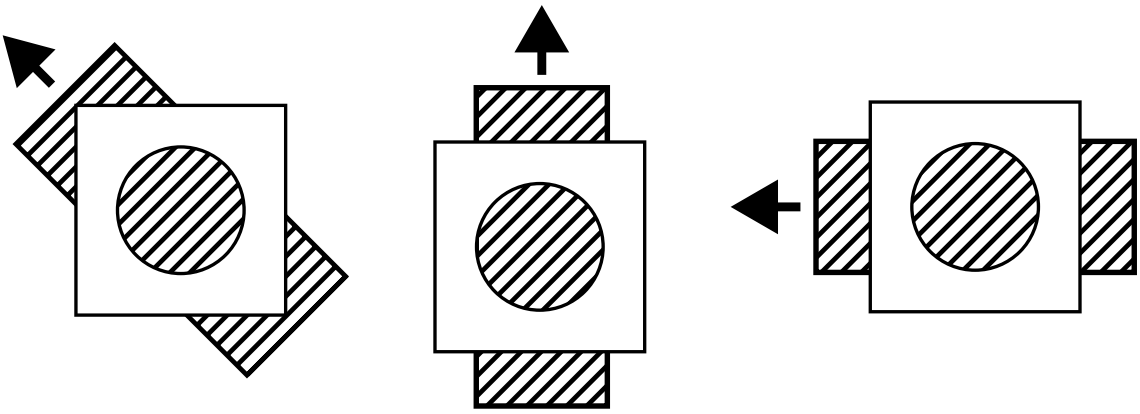

The motion of an oriented line is compatible with multiple global motion directions when viewed through an aperture. Since the small receptive fields of direction-selective cells act like apertures, the information that these cells can extract is inherently ambiguous. Adapted from Wolfe, Kluender, and Levi (2020).

Another layer of complexity in understanding motion integration is added by the computations performed by the visual system on this vector flow map. Not only does the visual system correctly determine which local cues belong together, such as in the detection of coherence (Adelson and Movshon 1982) or figure-ground segregation (Fahle 1993), but it also extracts a range of higher-level information from the flow map (for recent reviews, see Nishida et al. 2018; Park and Tadin 2018). This includes discerning the animacy (Scholl and Tremoulet 2000) and material properties (Doerschner et al. 2011) of moving objects. Extracting such high level information requires not only the spatiotemporal integration of local motion cues, but also the potential integration of motion information with other visual processes.

Finally, a third layer of complexity in motion integration stems from the existence of distinct motion perception systems that seem to work in parallel (Cavanagh 1992; Lu and Sperling 2001; Nishida et al. 2018). These motion perception systems can be broadly categorized into two groups based on their reliance on either the activity of direction-selective cells or attentive tracking of the position of visual fea-

tures (Cavanagh 1992; Lu and Sperling 2001). We will refer to these systems as the velocity- and position-based motion systems. Although there are exceptional cases where a specific motion can only be detected by a particular motion system, these two groups of systems often operate in parallel. For instance, the common type of motion involving the translational movement of an object can be detected by both direction-selective cells and the attentional tracking of object position. Given that these motion systems can independently extract motion information in parallel, the visual system must integrate information from these distinct systems or determine which information source to prioritize to generate a coherent perception of motion.

All these various aspects and stages involved in motion integration contribute to the complexity of investigating this topic. Previous research has dedicated significant efforts to understanding how the visual system addresses the aperture problem to estimate a flow map of local motion vectors (for a comprehensive review, see Nishida et al. 2018). Despite the significant progress made in comprehending motion integration at this stage, certain issues remain unresolved, such as the form-dependent pooling of direction-selective cells (Allard and Arleo 2021; Lorenceau and Alais 2001; McDermott, Weiss, and Adelson 2001). Additionally, substantial attention has been given to elucidating higher-level mechanisms of motion perception that are presumed to be computed based on the vector flow map extracted in earlier stages of motion processing. However, an overarching model that unifies the diverse phenomena belonging to this stage of motion processing is yet to be established. Furthermore, the interaction between different motion perception systems has received relatively little attention and warrants further investigation.

In summary, despite significant efforts and progress made in understanding the integration of motion information in the visual system, there is still much work to be done in order to gain a comprehensive understanding of this process. Therefore, the purpose of this thesis is to contribute to the existing knowledge through the two studies presented in the following chapters. The first study is a psychophysics investigation that explores how different motion perception systems bind moving visual features together and how the visual system handles discrepancies in motion information extracted by these systems (Chapter 2). The second is an EEG study that initially aimed to identify an electrophysiological marker of motion integration using SSVEPs. However, during our preliminary attempts, we discovered a previously unknown technical limitation associated with utilizing SSVEPs alongside moving stimuli. As a result, we shifted our focus to documenting this limitation and devising potential solutions. Thus, Chapter 3 outlines this issue and presents our proposed solution, with the hope that this work will facilitate the use of SSVEPs in future studies investigating motion perception.

2. DISTINCT RULES FOR BINDING IN POSITION-BASED AND VELOCITY-BASED MOTION SYSTEMS

2.1 Introduction

Motion perception is a complex process that requires the brain to disambiguate and integrate motion cues across both space and time. Moreover, these motion cues can occur within a wide range of spatial and temporal windows, requiring a great deal of flexibility in the spatiotemporal receptive fields of motion-sensitive units. In accordance with this inherent complexity of motion perception, previous literature proposed several motion perception systems to account for the various types of motion that can be detected by the visual system. These systems include first-order, second-order, and third-order motion (Lu and Sperling 2001), as well as feature tracking (Cavanagh 1992; Seiffert and Cavanagh 1998). While the existence of some of these systems remains a subject of ongoing debate (for comprehensive reviews, see Burr and Thompson 2011; Nishida 2011; Park and Tadin 2018), the literature converges on at least two distinct mechanisms on which motion perception depends: A short-range velocity-based motion system sensitive to local motion energy (Adelson and Bergen 1985; Watson and Ahumada 1985), and a long-range position-based system that tracks visual features across space and time (Cavanagh 1992; Lu and Sperling 2001). The velocity-based motion system is assumed to be facilitated primarily by direction-selective cells (Emerson, Bergen, and Adelson 1992) and it broadly encompasses phenomena traditionally categorized under first-order motion and certain types of second-order motion. The position-based motion system, on the other hand, is facilitated by attention (Cavanagh 1992; Lu and Sperling 2001), and it includes both the third-order motion system and feature tracking.

Early studies in motion perception focused on explaining phenomena that cannot be accounted by models of motion-detecting units (i.e., the Reichardt detector, and later the Fourier motion-energy models), and thereby outlined a number

of cases in which the motion perception is facilitated by specialized motion systems (e.g., Lu and Sperling 2001; Seiffert and Cavanagh 1999). Most notably, the insensibility of such motion detectors to chromaticity led to the formulation of the position-based motion system, which enables the perception of motion defined by equiluminant color contrast (Cavanagh 1992; Lu and Sperling 2001). Likewise, it has been shown that the motion of contrast-modulated texture gratings without net luminance differences is detected by the position-based motion system at low speeds and contrasts, but by the velocity-based system at high speeds and contrasts (Seiffert and Cavanagh 1999; cf. Allard and Faubert 2013*a*,*b*). While such cases posit that each system can process motion independently, most natural motion stimuli can be processed by both systems in parallel (Cavanagh 1992; Nishida et al. 2018). This raises the question of whether there could be discrepancies between the motion information extracted by the two systems when they process the same stimulus in parallel, and how the visual system handles such discrepancies if they do exist.

Previous studies have used stimulus modifications that selectively deactivated the two motion systems and revealed insights about how the two systems might process the same motion information differently (Allard and Arleo 2021; Allard and Faubert 2016; Pantle and Picciano 1976). For instance, Pantle & Picciano (1976) utilized the temporal limitations of short-range motion perception (inter-stimulus interval $\lessapprox$ 40 ms; Baker and Braddick 1985*a*,*b*; Georgeson and Harris 1990) to impair the velocity-based motion system and manipulated the temporal distance (i.e., inter-stimulus interval: ISI) between the two frames of a Ternus display. Their stimulus was bistable (i.e., element or group motion) when the ISI was approximately 40 ms, but the bistability diminished in opposite directions when the velocity-based motion system was involved versus when it was impaired (i.e., the dominant percept was different for ISI $>$ 40 ms versus ISI $<$ 40 ms). This contrast suggests that the two motion systems favor opposing perceptual alternatives of this particular bistable display, indicating that the two motion systems can potentially reach different perceptual decisions based on the same input. Another example comes from Allard & Faubert (2016) who argued that the perceptual differences observed between the central versus peripheral presentation of the furrow illusion (Anstis 2012) may instead be attributed to the differential processing of motion information by the two motion systems. The furrow illusion involves a dot moving vertically on a slanted grating, which produces an illusion of the dot moving at an angle when viewed in the periphery. This illusory motion is at odds with the dot's global motion, but compatible with its local motion energy (Anstis 2012). Previous accounts of the illusion argued that the perceptual susceptibility to the local motion energy in the periphery is due to a difference in how motion is processed in the peripheral versus

central vision (Anstis 2012). However, Allard & Faubert (2016) replicated the illusion in central vision by using crowding to disrupt the position-based motion system, indicating that the central versus peripheral difference in the illusion is instead due to a discrepancy in the motion information extracted by the two systems.

More recently, evidence suggests that not only the two motion systems can potentially reach different estimates of the same stimulus, but they also interact with each other to produce coherent motion perception. A study by Allard & Arleo (2021) found that judgments of the rotation direction of a circular arrangement of dots were more accurate when both motion systems were active, compared to when either of them was impaired. Critically, the involvement of the position-based motion system improved participants' accuracy even in a reverse-phi version of their stimulus, in which the velocity-based motion system would detect a motion in the opposite (and incorrect) direction. In contrast, when the number of the dots was increased beyond the limit of attentional resolution, thereby impairing the position-based motion system, participants consistently reported a rotation in the opposite, incorrect direction. This indicates that the visual system actively rectified the incorrect direction detection by the velocity-based motion system through the information from the position-based motion system.

Together, these findings suggest that (1) information from the two systems interact to produce motion perception, (2) the two systems can extract different motion information from the same stimulus, and (3) the conflicting information from the two systems can lead to bistability in certain circumstances. Moreover, recent findings point out the role of static, motion-independent stimulus properties in the differences between how the two motion systems bind moving features. Allard & Arleo (2021) used rotating shapes with occluded corners and selectively impaired the two systems to investigate how static form information (visible vs. invisible occluders) influences the binding judgments of each motion system. Accurately judging the rotation direction of such a display requires integrating the motion of local line segments, which was previously found to be only possible when the occluders were visible, indicating a form dependence in binding motion (Lorenceau and Alais 2001). However, Allard & Arleo (2021) found that form information affected the accuracy of rotation direction judgments only when the position-based motion system was involved, but not when the velocity-based motion system was the only active system. This finding suggests that static form cues are taken into account by the position-based motion system when binding local motion cues, but are disregarded by the velocity-based motion system (Allard and Arleo 2021). Thus, one potential reason for the emerging discrepancies between the two motion systems could be the distinct rules for binding in the velocity- and position-based motion

systems, especially when the static cues suggest a different binding configuration than the motion cues.

To investigate whether static cues influence the perceptual binding decisions of velocity- and position-based motion systems differently, we used a bistable motion stimulus consisting of four pairs of dots, each rotating around their shared center, positioned equidistantly around the fixation cross (Figure 2.1a; Anstis and Kim 2011). This display stochastically elicits two different percepts at the viewer: Either as each dot rotating in tandem with its most proximate pair (i.e., local motion; Figure 2.1b), or moving around the fixation cross as the corners of two illusory squares (i.e., global motion; Figure 2.1c). Manipulating the distances within- and between dot pairs, as well as cueing different percepts through contrast groupings are known to moderate the probability of each percept (Anstis and Kim 2011; Zharikova, Gepshtein, and van Leeuwen 2017), indicating an influence of grouping principles such as proximity and similarity. Nevertheless, the probabilities of perceiving the two alternative percepts do not perfectly follow Gestalt principles as the global motion still dominates at proximity configurations that should favor the local motion more (Zharikova, Gepshtein, and van Leeuwen 2017). If the static cues are important for the position-based motion system but not for the velocity-based system, impairing the velocity-based motion system should make static cues more influential in determining how the individual moving dots will be grouped. To test this hypothesis, we used contrast groupings to cue global and local percepts through similarity, and incrementally increased the spatiotemporal distance between each frame of our motion display. Since direction-selective cells have short temporal windows (<100 ms, adaptive to stimulus properties; Bair and Movshon 2004) and spatially constrained receptive fields (Hubel and Wiesel 1962, 1968), the latter manipulation systematically impairs the velocity-based motion system (Allard and Arleo 2021).

Figure 2.1 Bistable motion display

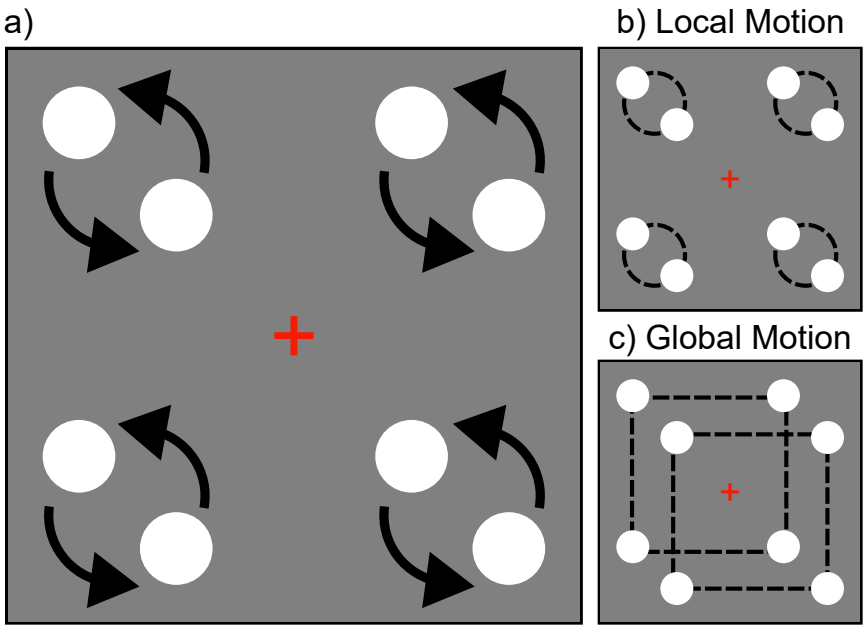

a) Bistable motion stimulus composed of four pairs of dots rotating around each other (Anstis and Kim 2011). The arrows indicate the rotation of the dot pairs. This display can induce two distinct percepts in the viewer: b) each dot rotating synchronously with its nearest pair, or c) the dots moving along the corners of two illusory squares. Dashed lines are included for illustrative purposes only.

2.2 Method

2.2.1 Participants

A total of 22 students (16 female, 6 male; mean age = 21.86 years, SD = 1.86) from Sabancı University participated in the study and received course credits as compensation. All participants had normal or corrected-to-normal vision and signed informed consent prior to the experiment session. Three subjects were excluded from data analyses based on the criteria outlined in the Results, leaving data from 19 participants to be used in further analyses. The sample size was determined based on previous studies with similar methods (Anstis and Kim 2011; Zharikova, Gepshtein, and van Leeuwen 2017). All experimental procedures were reviewed and approved by the Sabancı University Research Ethics Council.

2.2.2 Apparatus and Stimuli

Psychopy (Peirce et al. 2019) software was used to generate all stimuli and an ASUS XG248Q monitor (size = 23.8, resolution = 1920x1080, refresh rate = 60 Hz) was used as the experiment display. Participants viewed the stimuli in a dark and quiet room from a 61 cm distance. The stimuli consisted of a bistable motion display (Anstis and Kim 2011) in which eight moving dots could either be perceived as rotating in tandem with their most proximate pair (local motion; Figure 2.1b), or revolving around the fixation cross as the corners of two illusory squares (global motion; Figure 2.1c). The dots had a diameter of 1° and rotated either clockwise or counter-clockwise on a gray background (50% contrast). Each dot pair was distributed equidistantly around the fixation cross with an eccentricity of 5°. The center-to-center distance within each of the four dot pairs was 2°, whereas the distance between adjacent corners of the illusory squares extended 7°. Note that the distances within and between the dot pairs favored the local motion over global motion in terms of proximity as the dot pairs were closer to each other than the corners of the squares.

In two separate conditions, we cued local or global motion using contrast groupings. In the local-group condition, we presented the dots as either white or black, so that the dots had the same contrast polarity as their pairs, but an opposite contrast polarity with the adjacent corners of the illusory squares (Figure 2.2a). In the global-group condition, the corners of the two illusory squares had the same contrast polarity, but the dots were now of a different contrast polarity than their local pairs (Figure 2.2a). We expected these contrast pairings to respectively bias the bistable perception toward local and global motions through similarity, as has previously been demonstrated (Anstis and Kim 2011). We also included a third, no-group condition in which all dots were white as a neutral condition in terms of similarity. Therefore, we had three contrast grouping conditions in total: no-group, local-group, and global-group.

In addition to contrast groupings, we also manipulated the temporal distance between each frame of the motion display by displaying an empty screen (with the same background color) between the motion frames, which constituted our inter-stimulus intervals (ISI). The duration of these ISIs varied from 0 to 116.2 ms in steps of 16.6 ms (0 to 7 frames with a refresh rate of 60 Hz) in eight conditions (Figure 2.2b). This particular range of ISIs was chosen to encompass two important thresholds: 1) 40 ms, at which previous studies on short-range motion reported a limit for the velocity-based motion system (Baker and Braddick 1985*a*,*b*; Georgeson and Harris 1990), and 2) 100 ms, which is approximately the upper limit of tempo-

ral separation that can be integrated by direction-selective cells (Bair and Movshon 2004), although their temporal integration windows are also known to change duration adaptively according to stimulus properties (Bair and Movshon 2004). Overall, we expected increasing the ISI to impair the velocity-based motion system by preventing the direction-selective cells from detecting motion (Allard and Arleo 2021). Moreover, the movement speed of the dots was kept constant (1 cycle per second) across the ISI conditions by adjusting the movement distance between stimulus frames. This meant that the dots moved a greater distance at each stimulus frame when the ISI was larger. Since direction-selective cells have spatially constrained receptive fields (Hubel and Wiesel 1962, 1968), these larger spatial displacements were also expected to impair the velocity-based motion system.

Figure 2.2 Experimental conditions & design

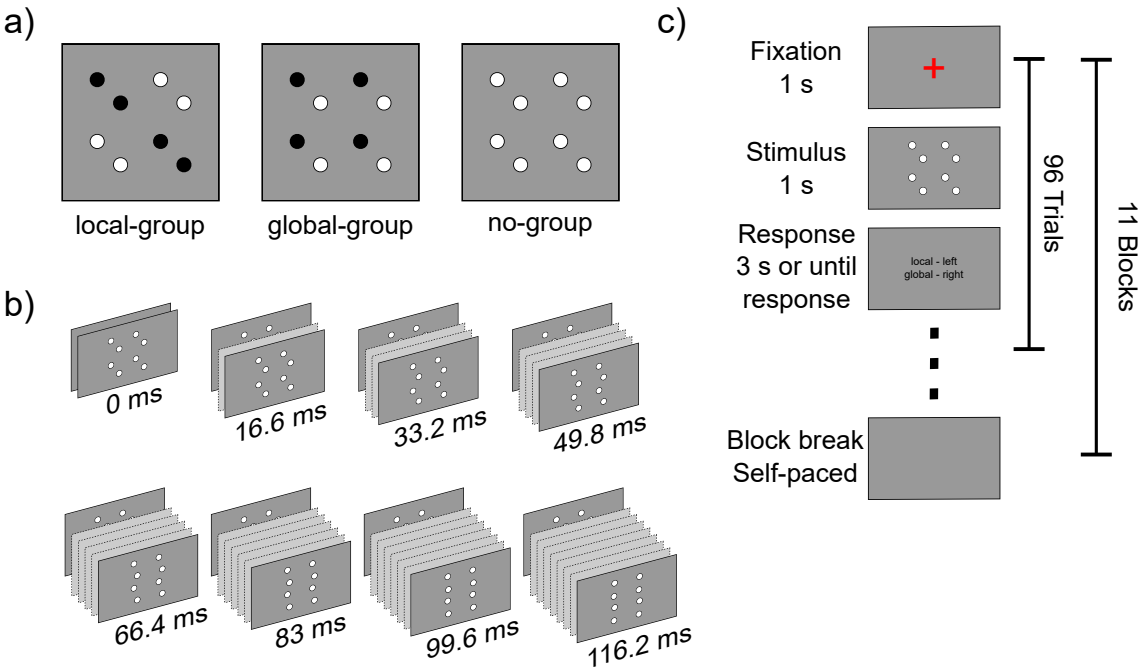

a) The three contrast grouping conditions: In the local-group condition, the dots within pairs shared the same contrast, cuing local motion. In the global-group condition, the corners of the illusory squares had the same contrast, cuing global motion. Neither percept was cued by contrast in the no-group condition, but the proximity cues favored local motion. b) The temporal distance (ISI) between each motion frame was manipulated by stroboscopically presenting empty frames between motion frames. There were 8 ISIs ranging from 0 to 116.2 ms, in steps of 16.6 ms. c) Each trial commenced with a 1-second fixation cross, followed by a 1-second stimulus presentation. Participants then reported their perceived motion type. The subsequent trial began immediately after participant response or after 3 seconds.

Together, the 3 contrast grouping and 8 ISI conditions led to 24 conditions in total. The experiment was segmented into 11 blocks of 96 trials, with 4 repetitions for each condition in each block. Trials from all conditions were presented in random order within each block. The first block acted as a training block to accustom participants to the task. Therefore, the trials from the first block were excluded from the data, leaving 40 trials per condition for the analyses.

2.2.3 Procedure

Prior to the experiment, participants were presented with visual guides illustrating the two motion percepts (local and global motion). The experiment did not commence until the participants reported clearly experiencing both percepts on a looped version of the motion stimulus. Each trial started with a 1-second presentation of a red fixation cross, and continued with the 1-second presentation of the motion display (Figure 2.2c). Participants were instructed to focus their gaze on the fixation cross. Immediately after the motion display, participants were prompted with an instructive text to indicate which motion they had perceived during the motion display by pressing keys on the keyboard. The text reminded participants of which key was associated with which percept (left arrow key for local motion, right arrow key for global motion), and remained on the screen for the whole response window of 3 seconds. If participants failed to respond within 3 seconds, a feedback text saying Too late! briefly appeared on the screen. The next trial automatically started upon response or at the end of the response window. Each block lasted approximately 4 minutes and participants took a self-paced break at the end of each block.

2.3 Results

For statistical testing, we calculated each participant's probability of seeing global motion (p_{global}) on each condition by dividing the number of trials where they reported seeing global motion by the total number of trials in that condition. We excluded the trials in which the participants failed to give a response. The number of such trials was minimal (max. 3 trials for any given condition, $M = 0.16$, $SD = 0.47$). Lastly, in order to remove outliers, we excluded the data from three participants whose p_{global} scores deviated from the sample mean by 2.5 standard deviations in at least one of the conditions.

Using Jamovi software (The jamovi project 2022), we conducted a 3-by-8 repeated-measures ANOVA (rm-ANOVA) on participants' p_{global} scores with contrast grouping (no-group, global-group, local-group) and ISI (0, 16.6, 33.2, 49.8, 66.4, 83, 99.6, 116.2 ms) as within-subject factors. A Greenhouse-Geisser correction was applied wherever the assumption of sphericity was violated. We found significant main effects of contrast grouping ($F(1.14, 20.54) = 56.99$, $p < .001$, $\eta^2_p = 0.760$) and ISI ($F(1.43, 25.71) = 58.81$, $p < .001$, $\eta^2_p = 0.766$), as well as a significant interaction between the two factors ($F(2.57, 46.32) = 9.82$, $p < .001$, $\eta^2_p = 0.353$). An analysis of the simple main effects revealed that ISI had a larger effect on the no-group ($F(7, 126) = 50.6$, $p < .001$, $\eta^2 = 0.738$) and local-group ($F(7, 126) = 37.41$, $p < .001$, $\eta^2 = 0.675$) conditions than on the global-group ($F(7, 126) = 14.74$, $p < .001$, $\eta^2 = 0.450$) condition. Figure 2.3 demonstrates that while p_{global} scores for the global-group condition were mostly stable across ISI levels, they showed a large deflection between ISIs of 16.6 and 33.2 ms for the no-group and local-group conditions. Bonferroni-corrected post hoc comparisons also revealed significant differences between ISIs of 16.6 and 33.2 ms for the no-group ($Mdiff = 0.27$, $p < .001$) and local-group ($Mdiff = 0.31$, $p = .002$) conditions. None of the other consecutive ISI levels within contrast grouping conditions differed significantly (all ps $> .05$). These results suggest a critical threshold for the velocity-based motion system at an ISI between 16.6 and 33.2 ms.

Bistable perception favored the global motion ($p_{global} > 0.5$) for ISIs shorter than 33.2 ms, even in the local-group condition, indicating that motion binding mostly disregarded the static cues at these ISIs. During smooth motion (ISI = 0ms), the no-group condition ($M = 0.70$, 95% $CI = [0.59, 0.80]$) did not significantly differ from both the local-group ($M = 0.59$, 95% $CI = [0.47, 0.70]$) and global-group conditions ($M = 0.89$, 95% $CI = [0.83, 0.96]$), whereas there was a significant difference between the local-group and global-group conditions ($p = .012$). At ISIs of 16.6 ms, however, the global-group condition ($M = 0.89$, 95% $CI = [0.82, 0.95]$) was significantly different than both the no-group ($M = 0.67$, 95% $CI = [0.57, 0.76]$) and local-group conditions ($M = 0.54$, 95% $CI = [0.44, 0.65]$). There was no significant difference between the no-group and local-group conditions at ISI = 16.6 ms ($p = 0.9$).

At ISIs equal to and larger than 33.2 ms, bistable perception started heavily favoring the local motion in the no-group ($M_{ISI \geq 33.2} = 0.21$, $SD = 0.12$) and local-group conditions ($M_{ISI \geq 33.2} = 0.17$, $SD = 0.11$), but not in the global-group condition ($M_{ISI \geq 33.2} = 0.70$, $SD = 0.23$). The global-group condition was significantly different than both the no-group and local-group conditions in all ISIs $\geq$ 33.2 ms (all ps $< .001$) while the no-group and local-group conditions did not

differ in any of these ISIs (all $ps > 0.4$). These results indicate that static cues had more influence on motion binding at ISIs $\geq$ 33.2 ms.

Figure 2.3 Probability of global motion across contrast grouping and ISI conditions

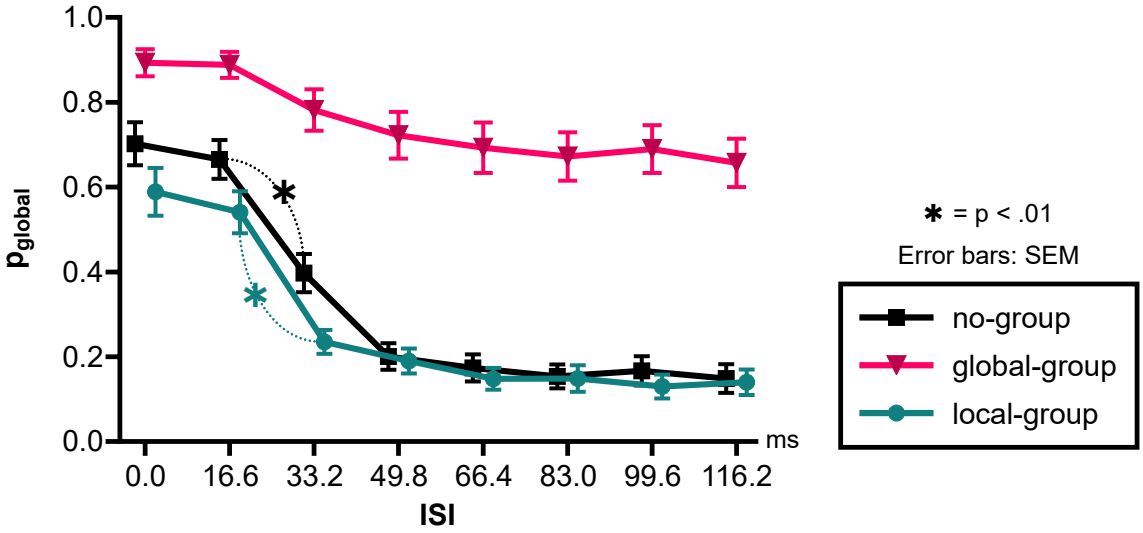

The probability of perceiving global motion (p_{global}) was determined by calculating the ratio of trials in which participants reported perceiving global motion to the total number of trials in each condition. Error bars represent the standard error of the mean. The figure omits the significant differences between contrast grouping conditions within the levels of ISI, for the sake of readability.

2.4 Discussion

We systematically impaired the contribution of the velocity-based motion system to the perception of a bistable motion display by increasing the duration of ISIs. Our findings revealed that at longer ISIs ($\geq$33.2 ms), static cues became more influential in how moving features were bound. We employed two conditions using contrast polarity to cue opposing perceptual alternatives of the bistable display (i.e., local vs. global motion) through similarity. Additionally, we had a third contrast grouping condition in which all individual features of the display had the same contrast polarity, yet was still configured to favor the local motion through proximity. At shorter ISIs ($<$ 33.2 ms), the global motion was the dominant percept even when the similarity and proximity cues favored the local motion. However, at longer ISIs, bistable perception was heavily biased toward the percepts favored by the similarity and proximity cues (i.e., global motion in the global-group condition, local motion

in the local-group and no-group conditions). These results indicate that static cues play a more important role in how the position-based motion system binds moving features. In contrast, the involvement of the velocity-based motion system seemed to counteract the binding configurations suggested by the static cues, as the global motion remained dominant at shorter ISIs regardless of similarity and proximity cues.

Our experimental design was based on a recent study by Allard & Arleo (2021), who examined the influence of form information on motion binding under normal and impaired velocity-based motion system conditions. Allard & Arleo (2021) employed a smooth motion condition (ISI = 0 ms) and a stroboscopic motion condition (ISI > 100 ms) to impair the velocity-based motion system by exploiting the temporal limitations of direction-selective cells (<100 ms). In comparison, we employed a range of ISIs to account for the previously reported threshold for short-range motion (40 ms; Baker and Braddick 1985*a*,*b*; Georgeson and Harris 1990) and to determine the specific point at which motion perception relies solely on the position-based motion system. Our findings indicate a temporal threshold for the velocity-based motion system between 16.6 and 33.2 ms, considerably shorter than the 40 ms threshold reported in previous studies. This shorter threshold might be attributed to an interaction between the spatial and temporal limitations of direction-selective cells, as we increased not only the temporal, but also the spatial distance of individual features between subsequent stimulus frames. Additionally, dynamic temporal integration windows of direction-selective cells, which depend on stimulus properties (Bair and Movshon 2004), could also potentially account for the shorter temporal threshold reported here. Nevertheless, it is important to acknowledge that our experimental design might have introduced perceptual biases that could have contributed to this temporal threshold shift.

In contrast to Allard & Arleo (2021), our study utilized a subjective measure of the content of perception, assessing the probability of alternative percepts in a bistable display, rather than an objective measure of perceptual accuracy. Since our task did not involve correct or incorrect responses, our data cannot be interpreted in light of factual information. This poses a challenge in determining whether the observed results stem from differences between the two motion systems or from unforeseen perceptual biases introduced by our experimental parameters. One potential factor to consider is the phenomenon of perceptual stabilization, where intermittent stimulus presentation can stabilize a bistable display across multiple trials (Leopold et al. 2002; Maier et al. 2003). Given that our experimental design involved relatively short trials and intertrial intervals, it is possible that perceptual content from previous trials influenced the perception of our bistable display in subsequent trials.

It is worth noting that there were more contrast grouping conditions favoring local motion (local-group and no-group) compared to global motion (global-group), which could have led to an overall bias toward perceiving local motion in the presence of perceptual stabilization. However, it remains unclear how this bias would differentially affect the three contrast grouping conditions across the various levels of ISI, as observed in our results. Crucially, all contrast grouping and ISI conditions were presented in a random order. Since all trials during perceptual stabilization could equally belong to any of the conditions, stabilization alone could not have selectively influenced specific conditions. Instead, perceptual stabilization might have resulted in a net bias toward the percept that presumably had a larger number of favorable trials, with the magnitude of bias likely dependent on the frequency and duration of stabilization. Thus, perceptual stabilization alone does not adequately explain the observed results.

The same considerations apply to other potential sources of bias in our study. Since our main finding is characterized by differences across the levels of both of our manipulations, our results are twofold. First, there is a distinction in the pattern of bistability between shorter (< 33.2 ms) and longer durations (≥ 33.2 ms) of ISIs. Second, the direction of bias is contingent upon the contrast grouping condition particularly at longer ISIs. Consequently, to account for our results, any potential bias would need to be sensitive to both the static cues and the duration of ISI. This implies that if we consider the smooth version of the stimulus (ISI = 0) as a baseline state, any presumed bias should only become noticeable at ISIs equal to or longer than 33.2 ms. Additionally, this bias should increase the probability of perceiving local motion in the local-group and no-group conditions while having minimal impact on the perception of the global-group condition. However, as we are not aware of a factor that meets these criteria, we contend that the most plausible explanation for our findings is a fundamental disparity in the binding rules employed by the two motion systems when integrating moving features.

Our findings reinforce existing evidence that the two motion systems are capable of extracting distinct motion information from the same visual input. This is evident in the substantial changes observed in the perception of our bistable display when the velocity-based motion system was impaired, leaving only the position-based motion system active, compared to when both systems were active. While our experimental design did not permit isolating the velocity-based motion system from the position-based motion system, the involvement of the velocity-based motion system appeared to introduce a general bias toward perceiving global motion. In contrast, when only the position-based motion system was active, bistable perception was primarily dominated by the percept favored by static cues. These findings

suggest that the velocity-based motion system binds moving features in a manner that places less or no emphasis on static cues.

Previous studies have strongly suggested that the position-based motion system is facilitated by a brain region located around the right inferior parietal lobe (IPL), which is associated with various functions related to temporal visual properties and temporal attention, aptly referred to as the "when" pathway of visual processing (Battelli, Pascual-Leone, and Cavanagh 2007). Lesions in this particular area have been shown to impair the position-based motion system while leaving the velocity-based motion system intact (Battelli et al. 2001), providing biological evidence for the functional dissociation between these two systems. Our stimulus' temporal properties were well within the previously reported 7 Hz temporal frequency limit of temporal attention for object tracking (Verstraten, Cavanagh, and Labianca 2000). This suggests that distinct visual pathways may be responsible for the different binding rules we observed for the two motion systems. If this is the case, it would be reasonable to assume that the "when" pathway leading to the right IPL might be responsible for the Gestalt-compatible binding patterns observed when the velocity-based motion system was impaired. On the other hand, the surround modulation mechanisms that aid in segregating moving surfaces in the hMT+ region (Er, Pamir, and Boyaci 2020; Tadin et al. 2003) would likely be responsible for the binding patterns observed when the velocity-based system was involved. However, further research is required to fully elucidate the exact contributions of these pathways and their interplay in motion perception.

The existence of different binding rules in the two motion systems raises the question of whether bistable motion perception arises from a conflict between the two motion systems. Previous research by Pantle and Picciano (1976) demonstrated that the two motion systems can extract opposing interpretations from the same motion stimulus, resulting in bistable perception under certain conditions. Therefore, it is possible that the bistability in our stimulus arises from a similar conflict, where each motion system extracts alternative percepts. However, the findings from our study contradict this perspective and suggest that the conflict between the two motion systems cannot solely account for the bistability inherent to our stimulus. This is evident from the fact that bistability did not completely disappear when the velocity-based motion system was impaired, although it was significantly reduced (with approximately 80% dominance for the percept favored by static cues). If bistability solely resulted from the conflict between the two systems, the stimulus would not exhibit bistability when only the position-based motion system was active. However, bistability persisted even after impairing the velocity-based motion system, indicating the presence of additional factors driving bistability within the position-

based motion system.

It remains uncertain whether separate factors driving bistability exist also within the velocity-based motion system. One possibility is that the observed bistability when both motion systems are active results from an overall bias toward global motion introduced by the velocity-based motion system, superimposed on the bistable perception originating from the position-based motion system. This would suggest that the specific pattern of bistability observed at shorter ISIs arises from an integration between the two motion systems, where the position-based motion system is primarily responsible for bistability while the velocity-based motion system may not exhibit bistability itself.

Alternatively, it is also conceivable that both motion systems possess distinct patterns of bistability: The bistability observed at shorter ISIs could represent either the integration of the two motion systems or solely the bistability originating from the velocity-based motion system, if perception at these ISIs is predominantly influenced by the velocity-based motion system. Further investigation is necessary to elucidate the precise mechanisms underlying the observed patterns of bistability and the respective contributions of the position-based and velocity-based motion systems.

In summary, our study provides evidence supporting the presence of distinct rules for binding moving features within the velocity-based and position-based motion systems. The position-based motion system predominantly relies on static cues, such as similarity and proximity, when integrating motion information. In contrast, the velocity-based motion system tends to disregard static cues, leading to binding configurations that may contradict those suggested by the static cues. These differential rules for motion binding in the two systems offer a potential explanation for the phenomenon of bistable perception in motion. However, our findings indicate that bistability exists independently within the position-based motion system for our specific stimulus, suggesting that bistability is not solely driven by a conflict between the two motion systems. It remains an open question whether bistability can also occur independently within the velocity-based motion system.

3. LARGE-SCALE CORTICAL DYNAMICS CAN PRODUCE MOTION-INDUCED SSVEPs

3.1 Background

One of the initial objectives of this thesis was to identify an electrophysiological marker of motion integration in the visual cortex. We recognized the potential of SSVEPs for this purpose. SSVEPs are periodic fluctuations in the EEG signal that correspond to periodic modulations in a stimulus property (Regan 1977). These fluctuations can be distinguished in the frequency domain as narrow-band frequency components. By representing the activity of neural populations sensitive to the modulated stimulus property, SSVEPs offer a robust means to track the activity of specific target populations.

Furthermore, a particular type of SSVEP component known as Intermodulation (IM) Components (Gordon et al. 2019) represents the activity of neurons that integrate input from different neural populations. IM components emerge when multiple visual features are modulated at distinct frequencies. Neural populations processing each visual feature generate SSVEP frequencies aligned with their respective modulation frequencies. Additionally, IM components manifest at frequencies that are specific combinations of two separate modulation frequencies. For example, if one visual feature is modulated at frequency *f1* and another at *f2*, IM components can be observed at the sum and/or difference of any integer multiples of *f1* and *f2* (e.g., $f1+f2$, $2f1-3f2$). Mathematically, these IM components can only arise from units that receive input from both neural populations, which themselves exhibit modulation at frequencies *f1* and *f2*, and compute a non-linear output based on their activity. Consequently, IM components serve as an objective marker of integrative activity in the brain, as evidenced by prior studies across various domains of visual perception, including face (Alp and Ozkan 2022; Boremanse, Norcia, and Rossion 2013), motion (Aissani et al. 2011; Alp et al. 2017), and symmetry perception (Alp

et al. 2018), as well as perceptual learning (Vergeer et al. 2018).

We wanted to leverage IM components to track the perceptual decisions of the visual system regarding the binding of moving features. To accomplish this, we employed the same bistable motion stimulus introduced in Chapter 2 (without contrast grouping and ISI manipulations) and modulated the luminance contrast of individual dots in the display at two different frequencies. The modulation frequency of each dot was configured in two different ways. In the first configuration, local dot pairs were modulated at different frequencies (12 and 15 Hz), while the dots at the corners of the two illusory squares were modulated at the same frequency (Figure 3.1a). We anticipated enhanced IM components when the local dot pairs were perceptually bound together (i.e., local motion). The second configuration was the opposite of the first (Figure 3.1b), and we expected enhanced IM frequencies during the perception of global motion.

Figure 3.1 Frequency configurations for the preliminary investigations

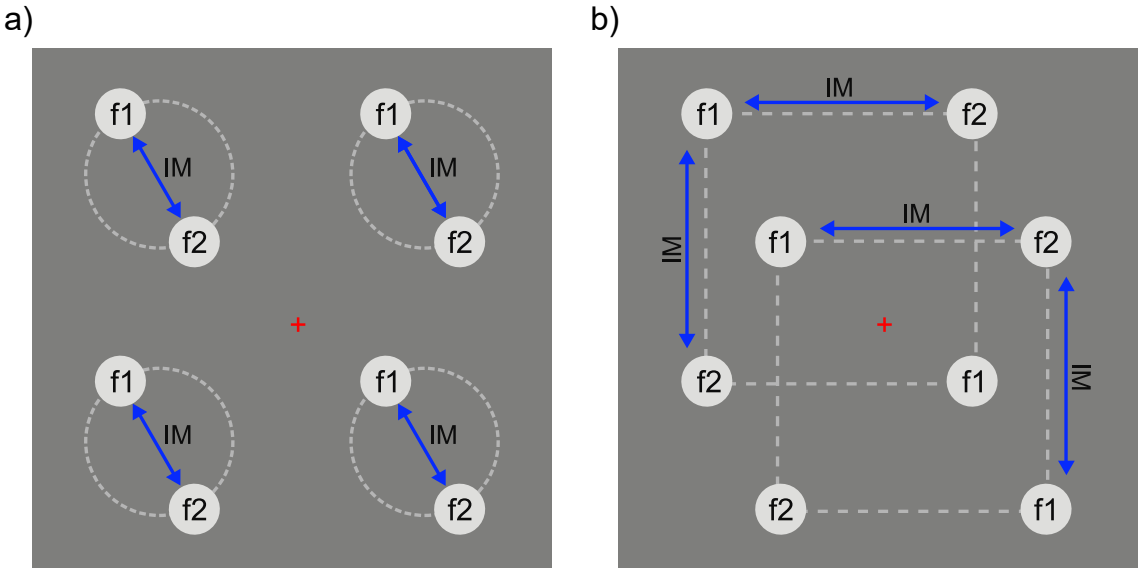

Frequency configurations used in the preliminary investigations. The individual dots in a bistable motion display were contrast-modulated at two different frequencies. The bistable display stochastically elicited two percepts in the viewers: local and global motion. During local motion perception, local pairs of dots appeared to be grouped together. During global motion perception, dots from each pair were grouped into two illusory squares. In (a), the modulation frequencies were configured so that the dots within local pairs would have different modulation frequencies, expected to produce IMs as a result of integrating local dot pairs. In (b) the corners of the illusory squares were modulated at different frequencies, expected to lead to IMs during global motion perception.

By utilizing IM components with such a bistable motion display, we aimed to establish an objective marker of the subjective perceptual decisions of the visual system. This was feasible because the stimulus remained physically unchanged while the perception of the stimulus continuously fluctuated between two percepts (i.e., local and global motion). Hence, any differences observed in the SSVEPs measured during local versus global motion perception could be attributed solely to the perceptual processes and not to differences in visual stimulation.

While the incorporation of a bistable stimulus represented a significant strength of this design, it also introduced a notable limitation. We lacked control over the duration and frequency of each motion percept, as perceptual switches occurred stochastically. Additionally, the frequency domain analyses necessitated long epoch durations, requiring the extraction of uninterrupted 10-second windows during each percept. These limitations resulted in a small and uneven dataset that was usable in our preliminary investigations involving 22 participants.

Moreover, our preliminary results revealed unexpectedly high signal-to-noise ratios for a number of frequencies that did not coincide with our modulation frequencies or the IM frequencies they could produce. Understanding the source of these unexpected frequencies was crucial for the progression of this study, as they had the potential to confound any subsequent experiments. Consequently, we directed our efforts toward explaining these frequencies and created simulations to depict how we expected our stimulus to modulate the activity of neurons in the early visual cortex. These simulations unveiled that the observed unexpected frequencies could not be generated by modulations in single-cell activity. Instead, our simulations suggested the existence of a large-scale factor that is able to influence the strength of population response based on the position of the stimulus. Building on these insights, we formulated a hypothesis that cortical magnification, a well-established structural characteristic of the visual cortex, could be responsible for generating these frequencies by modulating the EEG signal at different locations of the moving features in our stimulus.

3.2 Introduction

SSVEPs are periodic brain signals that occur in response to a periodically modulated stimulus property (Regan 1977). Specifically, when a stimulus property is modulated at a particular frequency, the activity of neurons that are sensitive to that stimulus property will also oscillate at analogous frequencies (i.e., fundamen-

tal modulation frequency and/or its harmonics). By utilizing stimulus presentation windows of sufficient length (e.g., t>1 second; Norcia et al. 2015) and employing frequency-domain analyses, these periodic oscillations can be precisely confined to narrow frequency bins. This property facilitates the isolation of visually evoked potentials from background noise, making SSVEPs a highly effective tool for a broad range of applications. These include, but are not limited to, assessing low-level sensory functions, such as contrast sensitivity (Allen, Tyler, and Norcia 1996; John et al. 2004), and establishing traceable neural signatures of high-level visual processes, such as face perception (Rossion et al. 2015; for an in-depth review for the applications of SSVEPs, refer to Norcia et al. 2015).

While SSVEPs induced by modulating stimulus properties are assumed to be related to the activity of neural populations sensitive to the modulated stimulus property, little consideration has been given to other factors that could potentially produce SSVEPs independently of neuronal activity. Since SSVEPs are produced by periodic fluctuations in the EEG amplitude, any factor that could influence the amplitude of the measured EEG signal would be capable of producing SSVEPs. In addition to synaptic activity, EEG amplitude can be influenced by morphological factors such as the size of the activated brain tissue (Schaul 1998), cortical depth of activated areas (Butler et al. 2019), cancellation between the simultaneous activity of different brain regions (Ahlfors et al. 2010), and thickness of the cerebrospinal fluid layer over regions of interest which can be influenced by participant posture (Rice et al. 2013). Although it is highly unlikely for these structural factors to periodically modulate the EEG amplitude in a time-locked manner across experimental trials, certain stimulus properties can conceivably have confounding interactions with the large-scale cortical dynamics of the visual cortex. For instance, the one-to-one mapping of the visual field to the visual cortex (i.e., retinotopic mapping; Allman and Kaas 1971; Daniel and Whitteridge 1961; Talbot and Marshall 1941; Wandell, Dumoulin, and Brewer 2007), and disproportionate allocation of brain tissue for processing different regions of the visual field (i.e., cortical magnification; Daniel and Whitteridge 1961; Horton and Hoyt 1991; Schwartz 1980) could result in stimuli retinal size and position influencing the EEG amplitude as a function of the size of the activated brain area. Consequently, a periodic modulation in stimulus size or position could lead to the large-scale cortical dynamics simulating SSVEPs by producing consistent fluctuations in the EEG signal, even in the absence of any modulation in the individual neuron responses.

One area of research that is particularly prone to such an interaction between stimulus properties and large-scale cortical dynamics is SSVEP studies involving moving stimuli. In motion SSVEP studies, the stimuli typically consist of visual

features that move across the visual field while a motion-related stimulus property is periodically modulated (e.g., Aissani et al. 2011; Alp et al. 2017; Pitchaimuthu et al. 2021; Varlet et al. 2023). Since early direction-selective cells are sensitive to velocity, luminance, and spatial frequency (Bair and Movshon 2004; Livingstone and Hubel 1988), it is reasonable to assume that modulating motion speed, motion direction, and luminance contrast can elicit fluctuations in the activity of early motion-sensitive populations. Moreover, higher-level motion-related stimulus properties processed in the extrastriate cortex such as pattern-motion (Huk and Heeger 2002), coherence (Braddick et al. 2001), and depth (Bradley and Andersen 1998) could also be employed to induce motion SSVEPs. Indeed, previous studies were able to observe motion-induced SSVEPs by modulating some of these low- and high-level stimulus properties. For example, Aissani et al. (2011) used bars that moved back and forth within a fixed distance, reversing their movement direction at a specific rate. They argued that this motion pattern would lead to SSVEPs at the direction-switch rate due to the fluctuating activity of direction-selective cells, which are known to respond maximally after a direction switch, with their response gradually fading out due to adaptation (Ales and Norcia 2009). In another study, Palomares et al. (2012) modulated the motion coherence of random dot kinematograms and observed SSVEPs at the coherence modulation rate, indicating that EEG amplitude is sensitive to motion coherence. Pitchaimuthu et al. (2021) used a singleton shape that moved along a horizontal axis on which the shape's position was determined by a sine function (i.e., simple harmonic motion), and observed SSVEPs at the frequency of the sine function. However, the sinusoidal modulation of the stimulus position in their design makes it difficult to identify the neural mechanisms that might have generated such SSVEPs, as the modulation also affects the shape's velocity and direction-switch rate as a side effect. Indeed, a recent study by Varlet et al. (2023) used a similar stimulus to compare two different velocity profiles (Sinusoidal vs. Rayleigh oscillations) and found phase differences between the responses evoked by the two velocity conditions, indicating that motion-induced SSVEPs can also be influenced by velocity.

These studies have illustrated the possibility of inducing SSVEPs by modulating stimulus properties to which motion-processing neural populations are sensitive. However, when the stimuli consist of non-stationary visual features, the retinal positions of the moving visual features are also modulated as a consequence of motion. This raises the question of whether a large-scale cortical dynamic such as cortical magnification could have contributed to the emergence of motion-induced SSVEPs. Cortical magnification could effectively lead to larger response amplitudes for the same stimulus when it is closer to the central visual field simply because

of the inverse relationship between stimulus eccentricity and the allocated area of the cortex processing that stimulus (Schwartz 1980). The same concept may also extend to polar angle-dependent asymmetries in cortical magnification (i.e., larger response amplitudes at specific polar angles; Adams and Horton 2003; Silva et al. 2018; Tootell et al. 1988; Van Essen, Newsome, and Maunsell 1984). If we conceptualize cells in the early visual cortex as units that produce an output based on visual information within their receptive fields, the effect of cortical magnification would be akin to increasing/decreasing the number of such units for each stimulus position. Even when these units are not sensitive to motion and therefore produce the same output regardless of motion-related stimulus properties, the aggregate activity from summed unit outputs would change as a function of position-dependent unit density. In this case, the periodicity observed in the signal would not be due to a modulation in the unit response, but rather to the non-uniform organization of the units. Moreover, this periodicity would be directly related to the modulations in motion-related stimulus properties such as speed or direction-switch rate as these properties are necessarily coupled to stimulus position. Consequently, this would mean that cortical magnification could independently lead to the same SSVEP frequencies the motion-processing populations are expected to produce, thereby posing a challenge for SSVEP studies attempting to isolate motion-specific activity from other visual processes.

To examine the hypothesis that cortical magnification could generate motion-induced SSVEPs independently of motion processing, we conducted two experiments. In Experiment 1, we investigated the effect of polar angle-dependent cortical magnification by presenting participants with a simple stimulus consisting of a single dot rotating around the fixation cross at a constant eccentricity. In Experiment 2, we used the same stimulus but modulated the dot's eccentricity to investigate the effect of eccentricity-dependent cortical magnification.

3.3 Experiment 1: Polar Angle Modulation

3.3.1 Method

Experiment 1 investigated whether modulation of stimulus polar angle could produce SSVEPs when other motion-related stimulus properties are kept constant.

3.3.1.1 Participants

14 Sabancı University students (8 female, 6 male; mean age = 21.1 years, *SD* = 2.02) with normal or corrected-to-normal vision participated in Experiment 1 for course credit. One participant's data was excluded from all analyses due to software errors during the recording session, reducing our sample size to 13. The sample size was based on previous studies with similar methods (e.g., Nozaradan, Peretz, and Mouraux 2012; Pitchaimuthu et al. 2021; Varlet et al. 2023. A sensitivity analysis conducted using GPower software (Faul et al. 2007) revealed that this sample size was sufficiently powered (power = .80) to detect large effect sizes (Cohen's f > .42) for our within-subjects factors (see, Frequency domain analysis). All procedures in this study were reviewed and approved by the Sabancı University Research Ethics Council. Participants gave informed consent prior to the experiment session.

3.3.1.2 Apparatus and stimuli

Stimuli were generated using Psychopy (Peirce et al. 2019) and presented on an ASUS XG248Q monitor (23.8, resolution=1920x1080) with a refresh rate of 60 Hz. Participants viewed the stimuli from a 76.5 cm distance in a dark and quiet room. The stimuli consisted of a single light gray (contrast = 75%) dot rotating around a fixation cross on a dark gray (contrast = 25%) background. The dot had a radius of 1° and an eccentricity of 5° from the fixation cross. The dot always completed one full rotation in exactly 1 second and had a constant movement speed with a 6° polar angle shift per motion frame. Trials lasted 11 seconds, during which the dot completed 11 full rotations.

The rotational motion of the dot meant that its polar angle was modulated as a function of time. The phase of this polar angle modulation depended on the position from which the dot started its rotation. In one condition, the dot's rotation always started from the same predetermined polar angle chosen randomly for each participant from a range of 0 to 350° in steps of 10 (e.g., 50° for one participant, 130° for another). The constant starting polar angle led to a phase-locked manipulation of the dot's polar angle across trials (Figure 3.2a). We will hereafter refer to this condition as the phase-locked (PL) condition. In the second condition, the starting polar angle was randomly selected for each trial from the same range (0 to 350° in steps of 10) without replacement (i.e., each step was used only once). Since the dot started its rotation from a different polar angle on each trial, the polar angle modulation was not phase-locked in this condition (Figure 3.2b). Therefore, we will

refer to this condition as the phase-varied (PV) condition. There were 72 trials for each phase condition (PL and PV).

Figure 3.2 Phase manipulation of the polar angle modulation

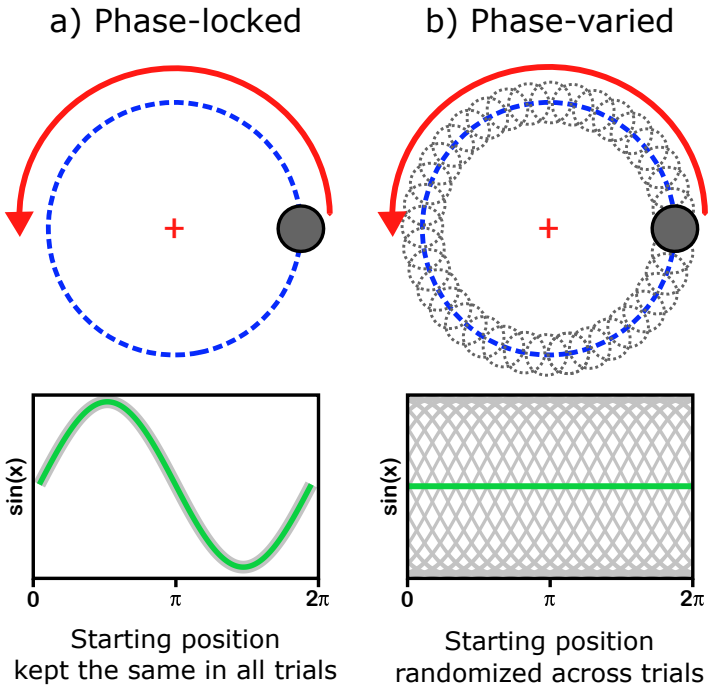

a) In the phase-locked condition, the dot consistently initiated its rotation from the same polar angle across trials, resulting in a consistent phase for the polar angle modulation. The sine functions in the second row are provided for illustrative purposes, demonstrating how the dot's starting angle influences the phase of the polar angle modulation. Although the actual shape of the signal evoked by the polar angle modulation may not be sinusoidal, its phase is expected to align with the phase of this modulation. b) In the phase-varied condition, the dot's starting angle was randomly chosen on each trial from 36 polar angle increments. Consequently, the polar angle modulation was not phase-locked across trials in the phase-varied condition, which would result in non-phase-locked signals canceling out each other when averaged in the time domain (the green straight line).

The only difference between the two phase conditions was the varied vs. locked phase of the polar angle modulation. All other stimulus properties, including motion speed, direction-switch rate, rotational frequency, and eccentricity were identical between the two conditions. Moreover, these properties were either not expected to produce SSVEPs as they were not periodically modulated (e.g., motion speed) or were expected to produce SSVEPs in both conditions as their modulations were phase-locked in all trials (e.g., direction-switch rate, rotational frequency). For example, even when the dot started its rotation from different angles, it repeated

its rotation cycle at exactly 1-second intervals (i.e., rotational frequency). Likewise, the dot's movement direction was shifted by the same amount at each frame regardless of its starting polar angle (i.e., direction-switch rate). Therefore, we expected any differences between the SSVEPs extracted from the two phase conditions to be caused specifically by the phase manipulation of the polar angle modulation. Since we were interested in EEG activity sensitive to polar angle modulation, we expected rotation direction to be a defining factor in the shape of the modulated EEG signal. Therefore, we also manipulated the rotation direction of the dot. In both phase conditions, the dot rotated either clockwise (CW) or counterclockwise (CCW), counterbalanced within each condition. Hence, we had 36 CW and 36 CCW trials for each phase condition.

3.3.1.3 Procedure

Each trial started with a fixation cross displayed on a gray background for 1 second, followed by an 11-second presentation of the rotating dot stimulus. After each trial, there was a self-paced break in which the participants pressed a keyboard key to proceed with the next trial. In approximately 14% of the trials (12 trials per block), the rotating dot briefly changed its color for 250 milliseconds at a random time (except during the first and last seconds of the trial). Participants were instructed to fixate on a red cross at the center of the screen, and press keys on the keyboard whenever they noticed a change in the dot's color (F key if the dot turned red, J if it turned green). The trial was terminated upon response or after the 1-second response window, with a feedback (i.e., correct/incorrect) text displayed for 1 second. These trials acted as catch trials to motivate participants to pay attention to the stimulus.

Trials from PL and PV conditions were presented in two separate blocks, the order of which was counterbalanced between participants. Each block consisted of 72 experimental and 12 catch trials, with an equal number of CW and CCW trials, in random order. Participants took a 3-5 minute break between the two blocks. Prior to the experiment, participants completed a short practice block (2-3 minutes) of 12 catch trials to get accustomed to the task.

3.3.1.4 EEG acquisition

EEG was recorded using 64 Ag/AgCl active electrodes placed on the scalp according to the international 10-10 system (ActiCAP, Brain Products GmbH, Gilching, Germany) with the following modifications: The channels TP10 and FT10 were placed above and below the participants' right eye to be used as vertical electrooculogram (VEOG) channels, and TP9 was used to replace the otherwise absent Iz channel. BrainVision Recorder software (Brain Products GmbH, Gilching, Germany) was used to record the EEG data at a 1000 Hz sampling rate with channel impedances kept below 20 kΩ.

3.3.1.5 EEG preprocessing

Fieldtrip Toolbox (Oostenveld et al. 2010) and custom scripts were used to preprocess the data in MATLAB (MATLAB 2021). A fourth-order Butterworth bandpass filter (0.5 - 100 Hz) was applied to the continuous data. Power line noise was removed by a multi-notch filter at frequencies 50, 100, and 150 Hz with bandwidths of 1, 2, and 3 Hz respectively. The online reference channel (FCz) was re-added to the data and channels were re-referenced to the average of all channels. Blink artifacts were removed by implementing an Independent Component Analysis (ICA) in Fieldtrip, using EEGLAB's runica algorithm (Delorme and Makeig 2004). Bad channels were determined by visual inspection and interpolated (0.37% per participant on average) using neighboring channels. Data were then segmented into 11-second trial epochs and downsampled by a quarter (250 Hz) for computational efficiency. A small number of trials were rejected ($M = 1.38\%$, $SD = 2.38$) due to hardware-related artifacts (peak amplitude > 500 µV). Data from the catch trials were excluded from all analyses.

3.3.1.6 Frequency domain analysis

We expected cortical magnification to induce periodic fluctuations in the EEG signal by modulating the strength of the population response at different polar angles of the rotating dot stimulus. Therefore, since the magnitude of cortical magnification depends on polar angle, the phases of these fluctuations are expected to align with the phase of our polar angle modulation. As a result, the fluctuations produced by cortical magnification are also anticipated to exhibit phase-locking across the trials of our PL condition, but not across the trials of the PV condition.

To extract these fluctuations induced by the polar angle modulation, we utilized time-domain averaging and averaged the trials from each of our conditions in the time domain (Trial $N \approx 36$). Time-domain averaging eliminates noise while keeping phase-locked signals intact (Trimble 1968). As a consequence, we expected time-domain averaging to preserve the polar angle modulation frequencies in the phase-locked condition, but eliminate the same frequencies in the phase-varied condition through phase-cancellation. As previously discussed (see, Apparatus and stimuli), other stimulus properties were either not expected to produce SSVEPs or were expected to produce SSVEPs in both conditions. Therefore, any frequencies with amplitudes significantly larger in the PL than the PV condition should belong to SSVEPs produced by the polar angle modulation alone.

We applied a Fourier transform on the time-averaged data (frequency resolution: $1/11 = 0.09$ Hz), and calculated the baseline-subtracted amplitudes by subtracting from the amplitude of each frequency bin the average amplitude of 16 neighboring bins (8 from both sides), with the exclusion of two immediately adjacent bins (one on each side). Since the dot's polar angle was modulated at 1 Hz, we expected to observe SSVEP frequencies at 1 Hz and its harmonics. We wanted to compare the overall amplitude of activity distributed across these fundamental and harmonic frequencies; therefore for statistical comparisons, we summed the baseline-subtracted amplitudes of all harmonic frequencies which were significantly above the noise level (Retter and Rossion 2016; Retter, Rossion, and Schiltz 2021). Significant harmonics were determined by first grand-averaging the FFT spectra across participants, channels, and conditions, and then calculating Z-scores for each frequency bin with a similar procedure to the baseline-subtracted amplitude calculation (i.e., 16 neighboring bins were used as the baseline for each frequency bin). Only SSVEP frequencies up to the sixth harmonic (including the fundamental frequency) passed the threshold of significance (Z-score > 1.64, $p < 0.05$, one-tailed, signal $>$ noise), and thus were included when calculating the summed baseline-subtracted amplitudes for each condition.

We identified two separate ROIs for our analyses. The first included only the Oz channel, which largely covers V1 where the properties of retinotopic organization and cortical magnification are most well-known (Dahlem and Tusch 2012; Daniel and Whitteridge 1961; Dow et al. 1981; Gattass, Sousa, and Rosa 1987; Palmer, Chen, and Seidemann 2012; Van Essen, Newsome, and Maunsell 1984). The second ROI consisted of 8 posterior channels (Oz, O1, O2, POz, PO3, PO4, PO7, PO8) which roughly encompass the occipital-parietal areas in which previous studies consistently found motion-induced SSVEP activity (Aissani et al. 2011; Alp et al. 2017; Nozaradan, Peretz, and Mouraux 2012; Palomares et al. 2012;

Pitchaimuthu et al. 2021; Varlet et al. 2023). Separately for each ROI, We ran a 2-by-2 repeated-measures ANOVA (rm-ANOVA) on participants' summed baseline-subtracted amplitudes with phase (PV vs. PL) and rotation direction (CW vs. CCW) as within-subject factors. For the first ROI, the summed baseline-subtracted amplitudes from the Oz channel were used in the rm-ANOVA. For the second ROI, we averaged the summed baseline-subtracted amplitudes from the 8 channels to quantify and compare the overall response in these posterior channels. All reported p-values for both tests were Bonferroni-corrected for multiple comparisons (i.e., one for each ROI; Keil et al. 2022). Lastly, we calculated the signal-to-noise ratio (SNR = signal/baseline) for all frequency bins using the same baseline as described above, to better illustrate the pattern of harmonic frequencies contained in the evoked signal. SNR is preferred for this purpose as higher frequencies can have a low amplitude (and therefore a low baseline-subtracted amplitude) but still have a high SNR.

3.3.2 Results

3.3.2.1 Behavioral results

The behavioral task in the catch trials served the sole purpose of encouraging participants to pay attention to the stimulus. Therefore, we only required participants to have accuracy above 50% on the catch trials. Overall, participants' accuracy was high ($M = 88.14\%$, $SD = 8.31$), and no participant had below-chance accuracy in either of the two experimental blocks (Min. = 58.33%).

3.3.2.2 Frequency domain results

Z-scores calculated on the grand-averaged amplitude spectra indicated that harmonics of the polar angle modulation frequency were significant up to the sixth harmonic (see Frequency domain analysis), thereby constituting our frequencies-of-interest for the following analyses. Figure 3.3 illustrates that these six frequencies are clearly distinguishable from noise in the two PL conditions (CW and CCW) whereas they are at noise levels (SNR ≈ 1) in the PV conditions. A visual inspection of the topographical maps (Figure 3.4) displaying the summed baseline-subtracted amplitudes for each condition across EEG channels suggests a clear posterior activity in the PL, but not in the PV, conditions.

Figure 3.3 FFT signal-to-noise ratio (SNR) spectra

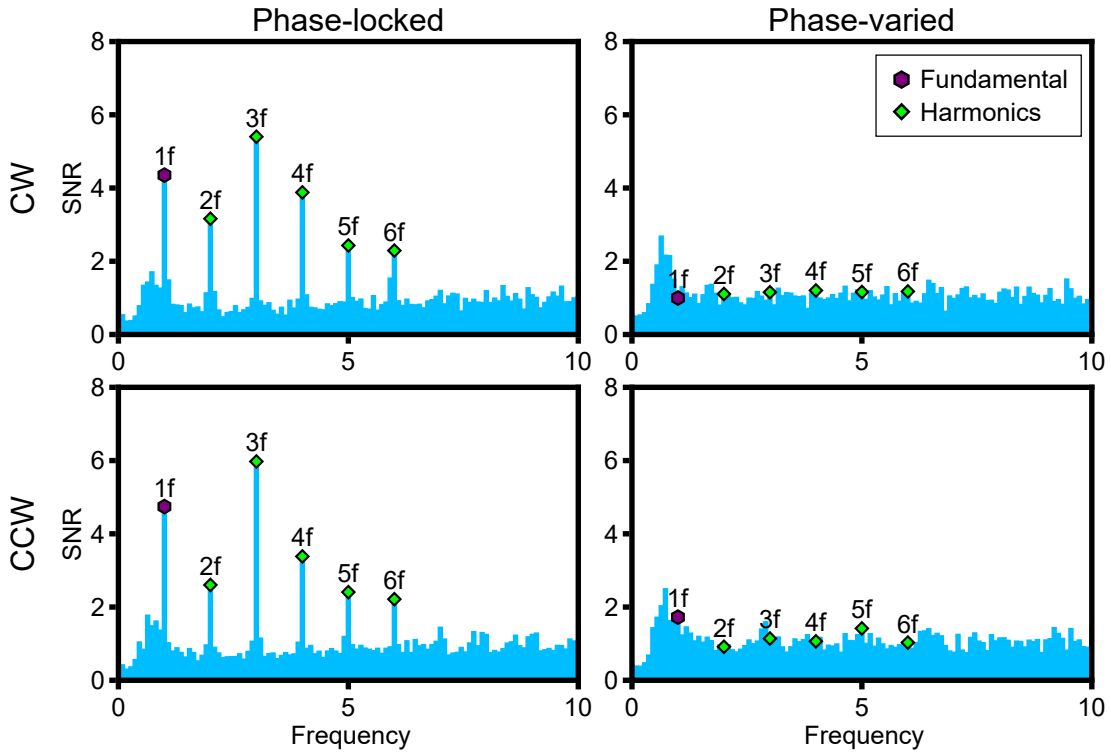

SNR calculated on the FFT amplitude spectra obtained from time-domain averaged trials for each condition. The figures here reflect the SNR values extracted from the Oz channel, averaged across participants. The first six harmonics of the modulation frequency ($1f$, $2f$, $3f$, $4f$, $5f$, and $6f$) exhibit high SNR (> 2) in the phase-locked conditions, but are at noise levels ($\approx$1) in the phase-varied conditions.

Figure 3.4 Topographical maps of summed baseline-subtracted amplitudes

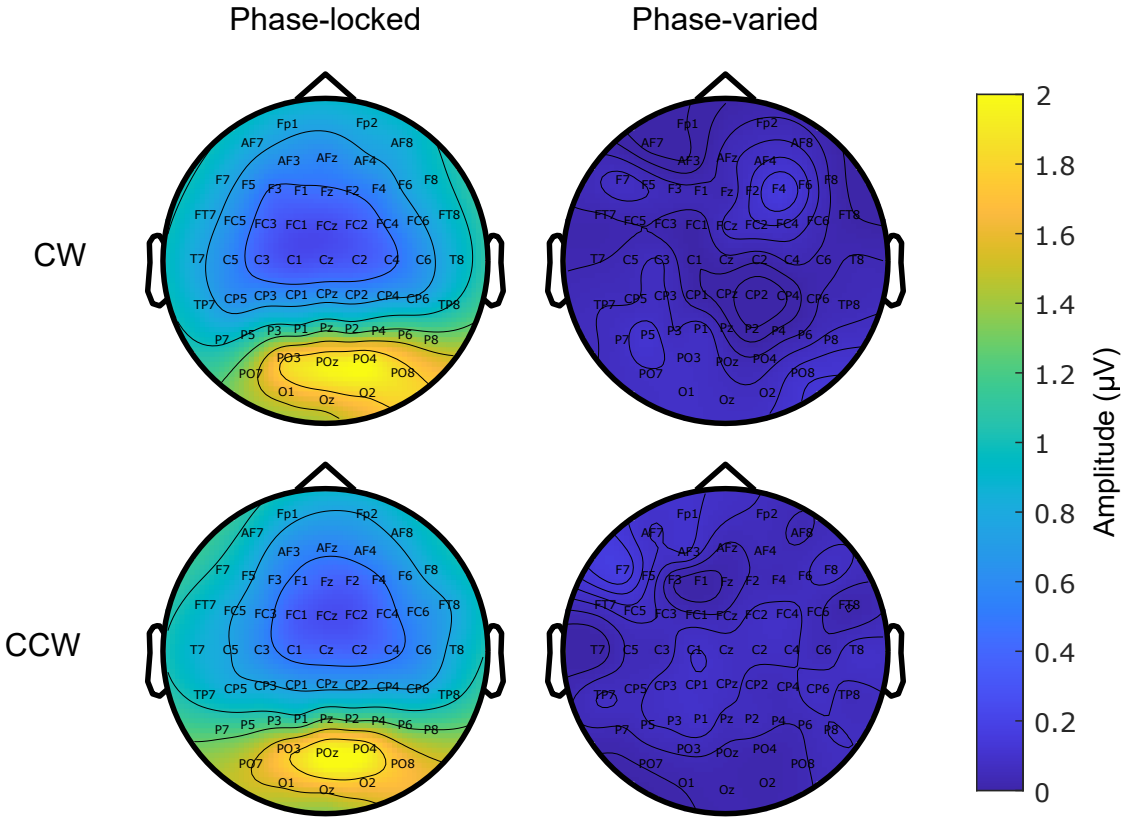

Grand-averaged summed baseline-subtracted amplitudes of the first six harmonics of the modulation frequency (1*f*, 2*f*, 3*f*, 4*f*, 5*f*, and 6*f*) across all channels.

A rm-ANOVA on the summed baseline-subtracted amplitudes from the Oz channel (i.e., the first ROI) revealed a significant main effect of phase ($F(1, 12) = 86.74$, $p_{bonf} < 10^{-5}$, $\eta^2_p = 0.878$). The main effect of rotation direction ($F(1, 12) = 0.59$, $p_{bonf} = 0.91$, $\eta^2_p = 0.047$) and the interaction term ($F(1, 12) = 5.86*10^{-5}$, $p_{bonf} = 1$, $\eta^2_p = 4.88*10^{-6}$) were not significant. Figure 3.5 depicts the distinction among each condition. Bonferroni-corrected post hoc tests revealed that the summed baseline-subtracted amplitudes from the PL condition were significantly larger than those from the PV condition, within both CW (*Mdiff* = 1.516, $p_{bonf} < 10^{-5}$) and CCW (*Mdiff* = 1.517, $p_{bonf} < 10^{-5}$) conditions. CW and CCW conditions did not differ significantly within PV (*Mdiff* = 0.048, $p_{bonf} = 1$) or PL (*Mdiff* = 0.047, $p_{bonf} = 1$) conditions.

Figure 3.5 Summed baseline-subtracted amplitudes

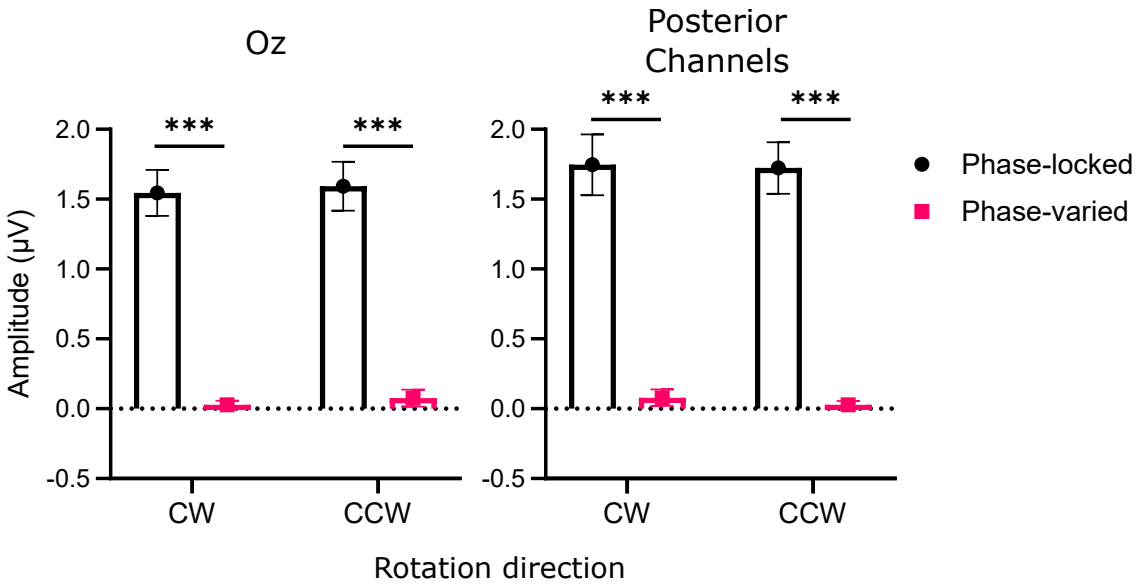

The summed baseline-subtracted amplitudes of the first six harmonics of the modulation frequency ($1f$, $2f$, $3f$, $4f$, $5f$, and $6f$) are depicted for the two regions-of-interest. Left: Summed baseline-subtracted amplitudes obtained from the Oz channel. Right: Average of the summed baseline-subtracted amplitudes obtained from the eight posterior EEG channels. Error bars indicate the standard error of the mean. Statistical significance is denoted as *** ($p < 10^{-5}$).

A separate rm-ANOVA on the summed baseline-subtracted amplitudes averaged from the eight posterior channels (i.e., the second ROI) also revealed similar results: The main effect of phase ($F(1, 12) = 75.77$, $p_{\text{bonf}} < 10^{-5}$, $\eta^2_{\text{p}} = 0.863$) was significant, but the main effect of rotation direction ($F(1, 12) = 0.48$, $p_{\text{bonf}} = 1$, $\eta^2_{\text{p}} = 0.039$) and the interaction term ($F(1, 12) = 0.064$, $p_{\text{bonf}} = 1$, $\eta^2_{\text{p}} = 0.005$) were not. The PL condition had larger summed baseline-subtracted amplitudes than the PV condition in both CW ($Mdiff = 1.67$, $p_{\text{bonf}} < 10^{-5}$) and CCW ($Mdiff = 1.69$, $p_{\text{bonf}} < 10^{-5}$) conditions (see Figure 3.5). There was no significant difference between the CW and CCW conditions within PV ($Mdiff = 0.05$, $p_{\text{bonf}} = 1$) or PL ($Mdiff = 0.023$, $p_{\text{bonf}} = 1$) conditions.

3.4 Experiment 2: Eccentricity Modulation

Results from Experiment 1 indicated that motion-induced SSVEPs depend on the phase of the polar angle modulation. These results are in line with our

hypothesis that polar angle-dependent cortical magnification can induce SSVEPs. Cortical magnification also depends on the eccentricity of the stimulus (Daniel and Whitteridge 1961; Horton and Hoyt 1991; Schwartz 1980). Therefore, in Experiment 2, we investigated the effect of eccentricity modulation on motion-induced SSVEPs.

3.4.1 Method

Materials and methods were identical to Experiment 1, with the exceptions outlined below.

3.4.1.1 Participants

13 Sabancı University students (8 female, 5 male; mean age = 21.38 years, $SD = 0.5$) with normal or corrected-to-normal vision were recruited in exchange for course credit. The sample size was based on previous studies as in Experiment 1. A sensitivity analysis revealed that this sample size was sufficiently powered (power = .80) to detect effect sizes larger than 0.73 (Cohen's d, one-tailed paired-samples t-test; see, Frequency domain analysis).

3.4.1.2 Apparatus and stimuli

In Experiment 2, we employed the same rotating dot stimulus but adjusted the position of the rotation trajectory by shifting it in eight different directions (shift direction angles: 0° to 315° in increments of 45°). As a consequence, the center of the rotation trajectory was always positioned 2° away from the fixation cross, which allowed the dot's eccentricity to be modulated between 3° and 7° during its rotation. The phase of this eccentricity modulation depended on the position from which the dot started its rotation. More specifically, the phase of the eccentricity modulation was determined by the relative angle between the dot's initial position and the axis of the trajectory shift (Figure 3.6). Using this property, we kept the phase of the eccentricity modulation constant across trials in the phase-locked (PL) eccentricity modulation condition and varied it in the phase-varied (PV) condition (range: 0° to 315° in steps of 45°; Figure 3.7). The constant eccentricity modulation phase used in the PL condition was randomized between participants by randomly assigning each participant a predetermined relative starting angle. This meant that the relative starting angle of the dot in the

PL condition, and therefore the phase of the eccentricity modulation, was different for each participant (but still stable across the PL trials within participants).

Figure 3.6 Rotation trajectory shift & the phase of the eccentricity modulation

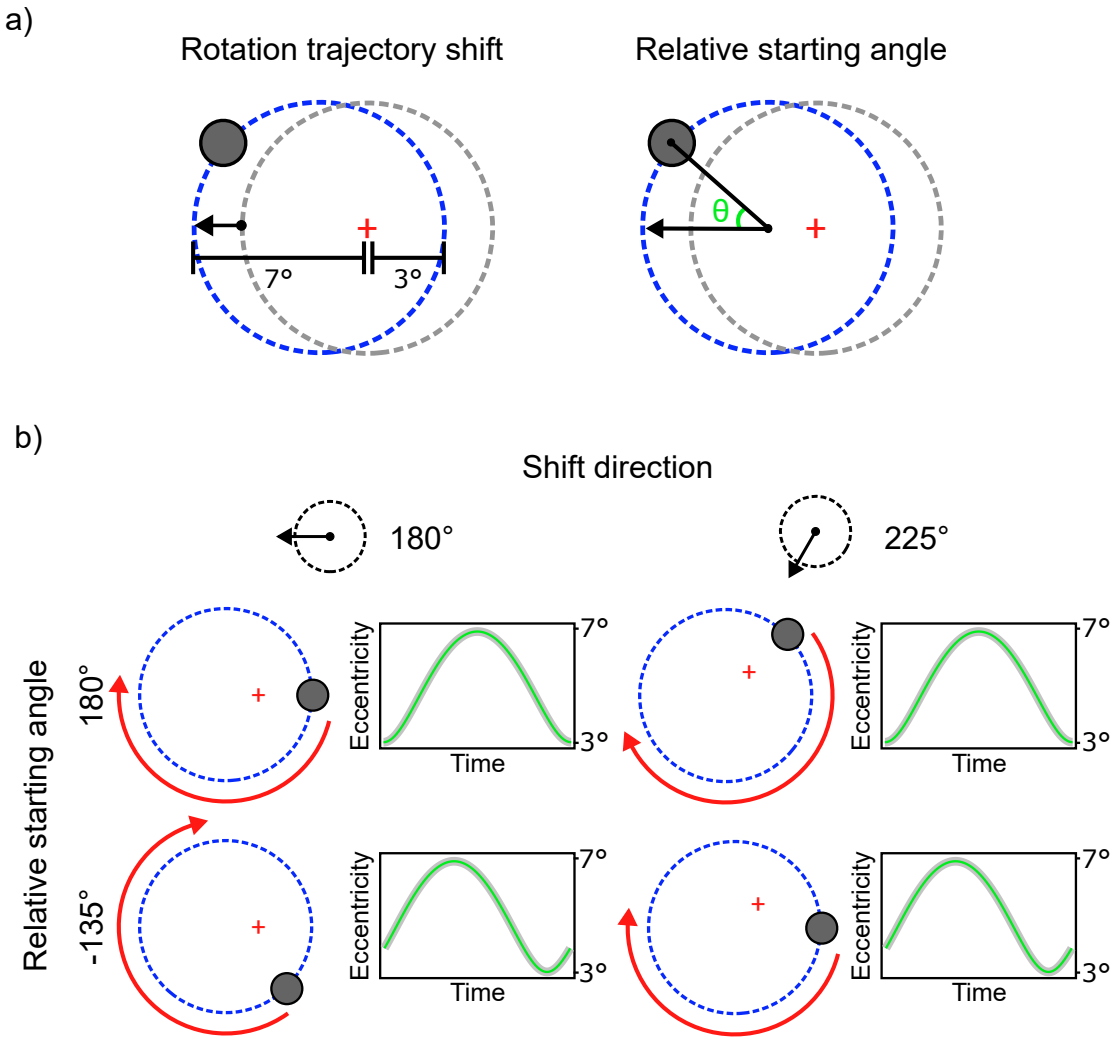

a) Left: The circular rotation trajectory was shifted by 2°. As a result, the dot's eccentricity changed from 3° to 7° during its rotation. Right: Relative starting angle of the dot defined as the angle between the vector of the rotation trajectory shift and the dot's initial position (shift direction angle - dot's polar angle). This relative starting angle determined the phase of the eccentricity modulation.
b) The phase of the eccentricity modulation was determined by the relative starting angle of the dot, even when different shift angles were applied to the rotation trajectories. The left and right columns represent conditions where the rotation trajectories were shifted in different directions, yet the phases of the eccentricity modulation remained the same. This consistency was achieved by maintaining the same relative starting angle across different shift directions.

Figure 3.7 Experimental design & conditions

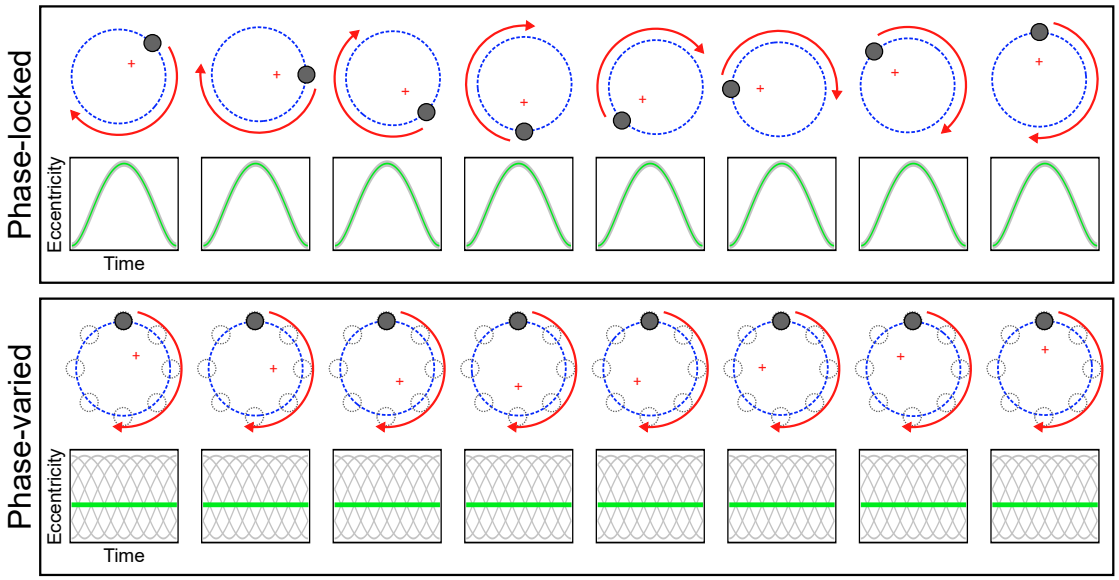

Phase-locked and phase-varied eccentricity modulation conditions in Experiment 2. Above: The circular rotation trajectory was shifted in 8 different directions, while the relative starting angle of the dot was kept constant to maintain a consistent phase of the eccentricity modulation across different shift directions. Below: The circular rotation trajectory was shifted in 8 directions, with 8 different starting positions for each shift direction, resulting in varied phases of the eccentricity modulation.

Shifting the rotation trajectory in eight different directions allowed for varying the phase of the polar angle modulation in both phase conditions, while still enabling a phase-locked eccentricity modulation in the PL condition. Therefore, we expected to observe only the SSVEPs induced by the eccentricity modulation, as those induced by the polar angle modulation would be eliminated through phase-cancelation. As a consequence of the cancellation of polar angle-dependent signals, any influence of the dot's rotation direction (CW and CCW) was also expected to be eliminated. Therefore, to increase the number of trials for our phase conditions, we omitted the rotation direction conditions in Experiment 2. Instead, we maintained a constant rotation direction (either clockwise or counterclockwise) across all trials, with the specific direction randomly predetermined for each participant.

Each trial lasted 10 seconds and contained 10 full rotations of the dot. Phase-locked and phase-varied conditions were presented in two different blocks similar to Experiment 1. Each block had 76 trials, 12 of which were catch trials. The task in the catch trials was identical to Experiment 1.

3.4.1.3 Frequency domain analysis

Bad channels were interpolated (0.5% per subject on average) using neighboring channels, and a small number of trials with hardware-related artifacts were excluded from the analyses (M = 0.96%, SD = 1.15). Later, trials from the PL and PV conditions were averaged separately in the time domain (Trial $N \approx 64$). Following the same Z-score calculation procedure and significance criterion as Experiment 1 (baseline: 14 neighboring bins for each frequency), only the fundamental frequency (1 Hz) was found significant. Therefore, we used the baseline-subtracted amplitudes of the fundamental frequency to compare the two conditions in two paired-samples t-tests for the two ROIs. Since we expected the PL condition to produce large baseline-subtracted amplitudes and the PV condition around the noise level (baseline-subtracted amplitude ≈ 0), we ran one-tailed tests.

3.4.2 Results

3.4.2.1 Behavioral results

Participants' accuracy on the behavioral task was similar to Experiment 1 (M = 84.62%, SD = 9.22, Min. = 58.33%).

3.4.2.2 Frequency domain results

Z-scores calculated on the grand-averaged amplitude spectra revealed that only the fundamental frequency was significantly larger than the noise (Z-score = 2.75, p = .003, one-tailed, signal > noise). Figure 3.8 shows that the fundamental frequency had a large SNR in the PL condition, but was at noise levels in the PV condition (SNR $\approx$ 1). Topographical maps of the baseline-subtracted amplitudes (Figure 3.9) suggest that phase-locked eccentricity modulation elicited activity in the posterior channels, whereas no particular activity was observed in the PV condition.

We ran two separate one-tailed (i.e., PL > PV) paired-samples t-tests on the two ROIs. The fundamental frequency had a significantly larger baseline-subtracted amplitude in the PL condition for both the Oz channel ($t(12) = 5.17$, $p_{\text{bonf}} < .001$, d= 1.43), and the average of the eight posterior channels ($t(12) = 5.12$, $p_{\text{bonf}} < .001$, d= 1.42), compared to the PV condition (Figure 3.9).

Figure 3.8 FFT signal-to-noise ratio (SNR) spectra

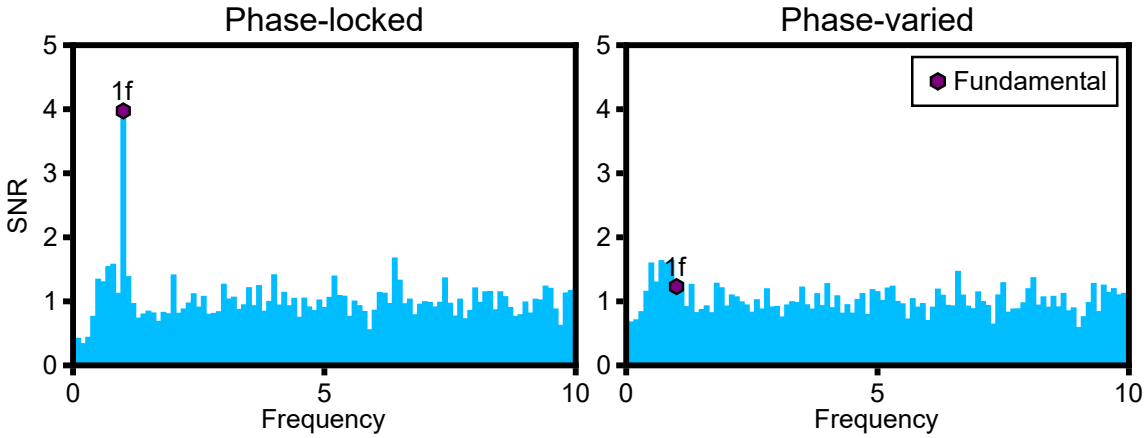

SNR calculated on the FFT amplitude spectra obtained from time-domain averaged trials for each condition, from the Oz channel. The fundamental modulation frequency (1f) exhibits a high SNR in the phase-locked condition, whereas its SNR is at noise levels in the phase-varied condition.

Figure 3.9 Topographical maps of baseline-subtracted amplitudes

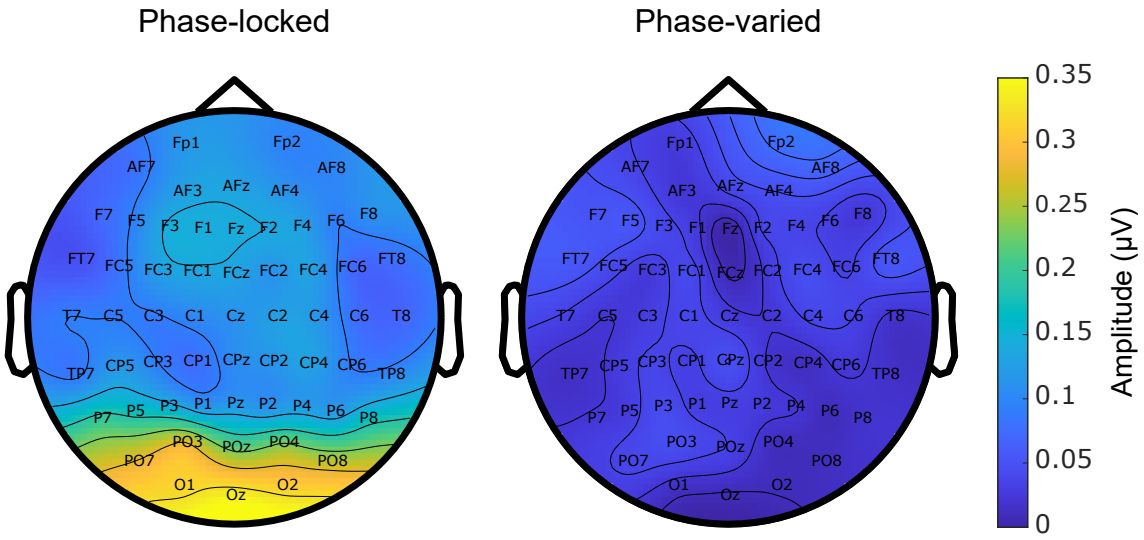

Grand-averaged baseline-subtracted amplitudes of the fundamental modulation frequency (1f) across all channels.

Figure 3.10 Baseline-subtracted amplitudes

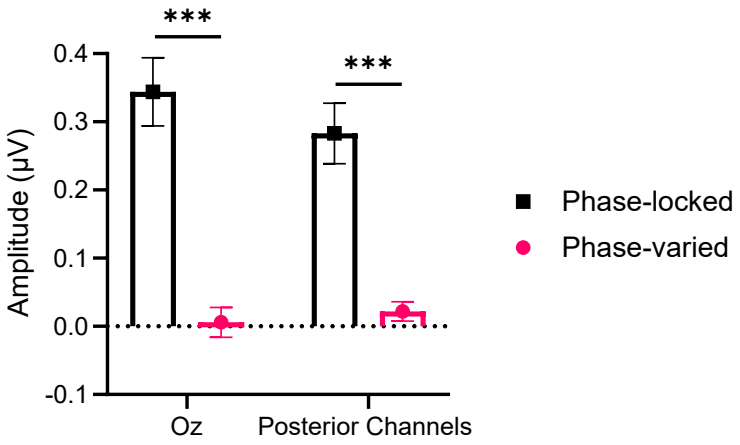

The baseline-subtracted amplitudes of the modulation frequency (1f) are depicted for the two regions-of-interest: Baseline-subtracted amplitudes obtained from the Oz channel, and average of the baseline-subtracted amplitudes obtained from the eight posterior EEG channels. Error bars indicate the standard error of the mean. Statistical significance is denoted as *** ($p < .001$).

3.5 Discussion

We hypothesized that large-scale position-dependent cortical dynamics could independently facilitate SSVEPs, irrespective of modulations in cell activity. Specifically, we anticipated that cortical magnification would modulate the EEG signal by amplifying or attenuating the response amplitude based on the magnitude of cortical magnification at different retinotopic locations of the stimulus. Therefore, we based our experiments on the two factors that decide the magnitude of cortical magnification polar angle and eccentricity.

In two experiments, we manipulated the phase of polar angle (Experiment 1) and eccentricity (Experiment 2) modulations of a rotating dot while keeping all other stimulus properties constant. Both experiments involved the comparison of a phase-locked and a phase-varied condition. In the phase-locked conditions, the polar angle and eccentricity modulations were phase-locked across trials, whereas we randomized their phases across the trials of the phase-varied conditions. Our goal was to identify purely position-dependent SSVEPs by eliminating them through phase-cancellation. Interestingly, we observed clear SSVEPs at the modulation frequencies in both experiments when the phases of the polar angle and eccentricity modulations were kept constant. However, when the phases of these modulations

were randomized, the same frequencies appeared at noise levels.

SSVEP frequencies are known to exhibit a narrowband characteristic, necessitating a periodic modulation of visual properties at very specific frequencies. In our study, the only property that underwent periodic modulation was the position of the stimulus. All other stimulus properties, including those associated with stimulus motion, remained constant and unfluctuating throughout the trials, or were consistent across both the phase-varied and phase-locked conditions. Thus, if any of these properties had the potential to generate SSVEPs, they would have been observed in both conditions. The absence of significant SSVEP frequencies in the phase-varied conditions, in contrast to the ones observed in the phase-locked conditions, suggests that phase randomization effectively canceled out these frequencies. This finding suggests that the neural activity responsible for generating the observed SSVEPs was specifically phase-locked to the modulations in stimulus position, highlighting a mechanism independent of motion-related properties but sensitive to stimulus position. To account for the observed SSVEPs, a position-dependent modulation of the EEG signal is necessary. These SSVEPs were most prominent in the early visual cortex, where individual cells operate on spatially fine receptive fields. Given the limited spatial extent of their receptive fields, it is unlikely for the cells in these early areas to have receptive fields large enough to modulate their response based on the position of our rotating dot stimulus. Instead, it is more plausible that the modulation in the EEG signal is influenced by factors that impact the strength of population response across different regions of the visual cortex. In this regard, cortical magnification emerges as a compelling explanation for our findings. The magnitude of cortical magnification is determined by retinotopic location, which subsequently impacts the size of the population responding to the same stimulus (Daniel and Whitteridge 1961; Horton and Hoyt 1991; Schwartz 1980). Hence, the position-dependent fluctuations observed in our study can be effectively attributed to variations in the size of neural populations responding to the rotating dot at different retinotopic locations, as determined by cortical magnification.

It is important to note that while our study's experimental design was based on known properties of cortical magnification, our results could also be explained by other large-scale population-level dynamics that can conceivably produce consistent position-dependent fluctuations in the EEG signal. Indeed, any number of factors that modulate the activity of retinotopically mapped neural populations could have driven the reported results, as long as the magnitude of their modulation varies across different retinotopic locations. While it might be possible to differentiate between the individual contributions of some of these factors, our experimental design does not permit making such distinctions. As a consequence, our findings cannot be

attributed solely to cortical magnification. Instead, the primary takeaway from this study should be that SSVEPs can arise not only from modulations in individual cell responses but also from broader mechanical, structural, and population-level dynamics. Nonetheless, considering the well-established properties of cortical magnification in the visual cortex, we posit that cortical magnification, as one of such dynamics, has likely played a role in producing these results.

One other noteworthy factor that may have driven our results is the presence of motion direction-dependent anisotropies in the visual cortex. Previous studies have demonstrated that motion directions radial to the fovea elicit larger brain responses compared to tangential directions (Clifford, Mannion, and McDonald 2009; Maloney, Watson, and Clifford 2014; Raemaekers et al. 2009; Schellekens et al. 2013). Specifically, these studies have reported a bias for centrifugal motion and a suppression of centripetal motion at lower stimulus eccentricities, while the opposite pattern was observed at higher eccentricities (Maloney, Watson, and Clifford 2014; Raemaekers et al. 2009). If such imbalances in responses to different motion directions were evident in our data, they could potentially account for some of our findings, particularly those from Experiment 2. Experiment 1, which exclusively involved tangential motion along the polar angle meridian, was not susceptible to the influence of motion direction anisotropies. However, in Experiment 2, due to the shift in rotation trajectory, the motion direction of the dot approximated radial motion at certain points, while being more tangential at other locations. These shifts in motion direction were also phase-locked to the eccentricity modulation, raising the possibility of confounding our phase manipulation. Nevertheless, the eccentricity range of our rotating dot spanned from 3° to 7°, encompassing the eccentricity threshold of approximately 5° where a complete reversal in the centrifugal versus centripetal bias was observed (Maloney, Watson, and Clifford 2014). This interaction between eccentricity and direction anisotropy would be expected to yield a more complex modulation of the EEG signal, with multiple even harmonics reflecting the axial symmetry caused by the reversal of the direction bias pattern (Figure 3.11). However, our findings revealed a linear response to our sinusoidal modulation of eccentricity, as indicated by the absence of harmonic frequencies in the signal. This sinusoidal response profile aligns better with the eccentricity-dependent variation in cortical magnification factors which decline linearly with increasing eccentricities (Dow et al. 1981; Schwartz 1980), lending greater support to cortical magnification as the primary explanation for our results. Nonetheless, additional research is needed to further disentangle the effects of motion direction anisotropy from those of cortical magnification.

Figure 3.11 Motion direction anisotropies & the eccentricity modulation

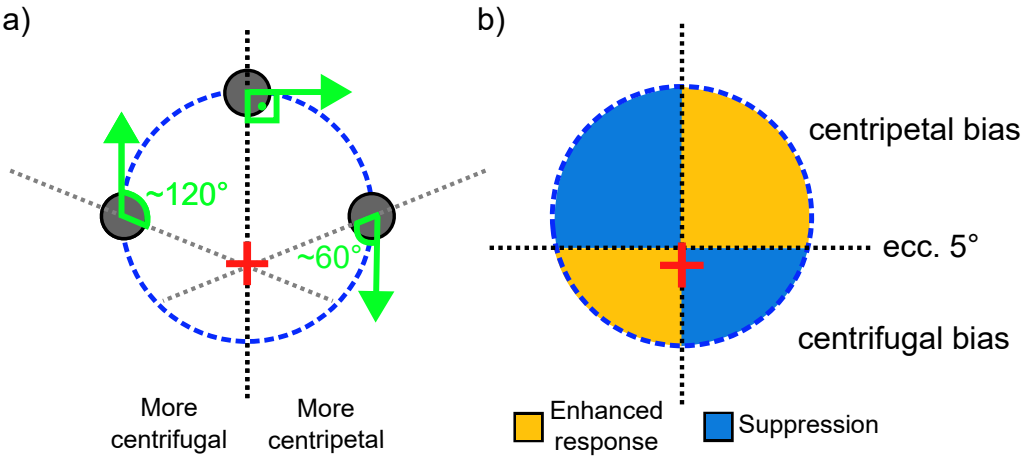

a) The motion direction of the dot approximates centrifugal motion when it is moving away from the fixation cross, and centripetal motion when it is moving toward the fixation cross. b) Motion direction anisotropies in the brain enhance responses to centrifugal motion at low eccentricities, and suppress them at high eccentricities. The threshold for this reversal ($\approx 5°$) falls within the range of our eccentricity modulation. As a result, we expect a symmetrical pattern of signal enhancement and suppression to emerge across the axes of the rotation trajectory. Such symmetrical response patterns are known to generate the even harmonics of the modulation frequency (Norcia et al. 2015).

Interestingly, while the eccentricity modulation led to a mostly linear response that contained only the modulation frequency ($f = 1$ Hz), the polar angle modulation produced complex SSVEPs that contained the first six harmonics of the modulation frequency ($1f$, $2f$, $3f$, $4f$, $5f$, and $6f$). This discrepancy can be attributed to the non-linear variation in cortical magnification factors with polar angle (Silva et al. 2018), unlike with eccentricity. Previous studies reported an intricate pattern of variation in cortical magnification factors as well as population receptive field sizes across different polar angles (Silva et al. 2018), and it is likely that this intricate pattern is responsible for the presence of multiple significant harmonics observed in Experiment 1.

The SSVEPs induced by position-dependent large-scale cortical dynamics, as demonstrated in our study, challenge the prevailing consensus that SSVEPs primarily arise from fluctuations in the responses of neurons processing a periodically modulated stimulus property. In our findings, the neurons contributing to the SSVEPs could be sensitive to any stimulus property, and yet generate the same SSVEP frequencies regardless of the specific processes they carry out. To illustrate this

point, let us consider hypothetical *roundness* detectors that could have responded to our dot stimulus. These fictitious roundness detectors would consistently respond whenever the dot falls within their receptive fields, without any fluctuations in their activity as the roundness of the dot remains constant. However, any variation in the density of these units across different retinotopic locations would result in differences in the population response measured at different positions of the dot, which would introduce periodic fluctuations in the signal. As a result, the observed SSVEPs would not provide insights into how these units process roundness, but rather reflect their structural organization in the brain.

Indeed, if we were to investigate these hypothetical roundness detectors and modulate the roundness of our rotating dot stimulus at a different frequency, we would be quite perplexed to observe significant harmonics of the rotational frequency. However, the disparity between SSVEPs produced by large-scale cortical dynamics and those generated by modulations in neuronal activity is not always readily apparent. As a consequence, SSVEP frequencies produced by large-scale cortical dynamics can be erroneously attributed to the activity of specific neural populations. In reality, any spatially heterogeneous populations of neurons would generate the same frequencies as long as they exhibit a steady response to the stimulus.

The contribution of large-scale cortical dynamics to SSVEPs might have already been overlooked in some studies. For instance, Pitchaimuthu et al. (2021) and Varlet et al. (2023) both used stimuli consisting of a singleton shape whose position along a horizontal trajectory was sinusoidally modulated. Notably, both studies observed significant SSVEPs at the frequency of the position modulation. Typically, such stimuli would be expected to generate even harmonics of the position modulation frequency, given the symmetrical characteristics of the motion. Specifically, the shape's motion direction switching twice within a motion cycle and the symmetrical velocity profile between the two halves of the motion trajectory would suggest SSVEPs at the even harmonics. In contrast, the existence of SSVEPs at the fundamental frequency indicates an activity sensitive to the periodicity or the beat of the motion (Nozaradan, Peretz, and Mouraux 2012; Pitchaimuthu et al. 2021; Varlet et al. 2023). Interestingly, we did not observe SSVEPs related to periodicity in our phase-varied conditions, even though the rotational motion cycle was repeated at consistent time intervals. In these trials, the dot completed a full cycle every 1 second, regardless of its starting position. If periodicity alone could induce SSVEPs, we would have expected to observe them in our phase-varied conditions as well. Instead, we only observed significant SSVEP frequencies when the polar angle and eccentricity modulations of the stimulus were phase-locked across trials. This

indicates that these SSVEPs were not driven by a motion-related property such as the motion cycle, but rather by the modulations in stimulus position. Therefore, it is possible that large-scale cortical dynamics played a role in facilitating the reported SSVEPs in these previous studies due to the modulations in polar angle and eccentricity of the stimulus.

One of the key advantages of SSVEPs is the ability to isolate and track the activity of specific neural populations. However, achieving this requires careful consideration of the targeted neural populations that will be influenced by experimental manipulations. Our study highlights a scenario in which SSVEPs do not reflect the activity of a specific population of neurons, but instead capture the broader structural dynamics of the visual cortex. If not adequately addressed in the experimental design, these large-scale cortical dynamics can introduce confounding factors that may lead to the misinterpretation of SSVEP frequencies, particularly in the context of moving stimuli. Furthermore, they can also lead to misleading amplitude differences in responses to different stimuli if those stimuli are consistently positioned at different retinotopic locations.

To mitigate these issues, we propose that researchers should give due consideration to these large-scale cortical dynamics when designing SSVEP studies. It is crucial to ensure that stimuli being compared do not have consistent differences in retinotopic position. Furthermore, in experiments involving moving stimuli, it is essential to clearly distinguish between SSVEPs generated by large-scale cortical dynamics and those arising from other visual processes. In our own experiments, we manipulated the phase of position modulations while keeping the phase of motion-related stimulus properties constant. This enabled us to eliminate the SSVEPs produced by position modulation through phase-cancellation. Future studies can employ similar approaches to effectively isolate the main activity of interest from the influence of large-scale cortical dynamics.

4. GENERAL DISCUSSION & CONCLUSION

The integration of motion information presents a complex and challenging task. The aim of this thesis was to advance our understanding of how the visual system accomplishes this task. The first study focused on investigating the principles underlying the binding of moving features by distinct motion perception systems, using a bistable motion display. Our findings revealed that the position-based motion system, which relies on attentive tracking of object positions, binds moving features based on grouping configurations indicated by static cues such as proximity and similarity. On the other hand, the velocity-based motion system, which relies on direction-selective cells, largely disregards these static cues when binding motion. This discovery of different integration rules followed by these two systems constitutes a novel contribution of this study. Additionally, our results support previous findings that these motion systems can extract substantially different motion information from the same stimulus. Notably, the observed differences in bistability patterns when both motion systems were active versus when only the position-based motion system was active suggest that the visual system integrates information from multiple motion systems to generate a coherent perception of motion.

The second study, while not directly contributing to our understanding of motion integration, highlights a significant limitation of the SSVEP methodology. We discovered that large-scale cortical dynamics can generate SSVEPs that mimic those produced by motion-sensitive neural populations as a byproduct of position modulation of moving stimuli. This finding raises concerns about previous studies that have utilized SSVEPs in conjunction with moving stimuli and attributed their results to motion integration, as they may have been confounded by the influence of large-scale cortical dynamics. To address this issue, we proposed a solution of randomizing the phase of position modulations across trials to eliminate SSVEPs generated by large-scale cortical dynamics. These technical advancements have the potential to improve the application of SSVEP methods in motion perception research, thereby contributing to the motion integration literature.

BIBLIOGRAPHY

Adams, Daniel L., and Jonathan C. Horton. 2003. "A Precise Retinotopic Map of Primate Striate Cortex Generated from the Representation of Angioscotomas." *Journal of Neuroscience* 23(May): 3771–3789.

Adelson, E. H., and J. A. Movshon. 1982. "Phenomenal Coherence of Moving Visual Patterns." *Nature* 300(December): 523–525.

Adelson, E. H., and J. R. Bergen. 1985. "Spatiotemporal Energy Models for the Perception of Motion." *Journal of the Optical Society of America. A, Optics and Image Science* 2(February): 284–299.

Ahlfors, Seppo P., Jooman Han, Fa-Hsuan Lin, Thomas Witzel, John W. Belliveau, Matti S. Hämäläinen, and Eric Halgren. 2010. "Cancellation of EEG and MEG Signals Generated by Extended and Distributed Sources." *Human Brain Mapping* 31(1): 140–149.

Aissani, Charles, Benoit Cottereau, Guillaume Dumas, Anne-Lise Paradis, and Jean Lorenceau. 2011. "Magnetoencephalographic Signatures of Visual Form and Motion Binding." *Brain Research* 1408(August): 27–40.

Ales, Justin M., and Anthony M. Norcia. 2009. "Assessing Direction-Specific Adaptation Using the Steady-State Visual Evoked Potential: Results from EEG Source Imaging." *Journal of Vision* 9(July): 8.

Allard, Rémy, and Angelo Arleo. 2021. "The False Aperture Problem: Global Motion Perception without Integration of Local Motion Signals." *Psychological Review* .

Allard, Rémy, and Jocelyn Faubert. 2013*a*. "No Dedicated Second-Order Motion System." *Journal of Vision* 13(September): 2.

Allard, Rémy, and Jocelyn Faubert. 2013*b*. "No Second-Order Motion System Sensitive to High Temporal Frequencies." *Journal of Vision* 13(April): 4.

Allard, Rémy, and Jocelyn Faubert. 2016. "The Role of Feature Tracking in the Furrow Illusion." *Frontiers in Human Neuroscience* 10.

Allen, D., C. W. Tyler, and A. M. Norcia. 1996. "Development of Grating Acuity and Contrast Sensitivity in the Central and Peripheral Visual Field of the Human Infant." *Vision Research* 36(July): 1945–1953.

Allman, J. M., and J. H. Kaas. 1971. "Representation of the Visual Field in Striate and Adjoining Cortex of the Owl Monkey (Aotus Trivirgatus)." *Brain Research* 35(December): 89–106.

Alp, Nihan, and Huseyin Ozkan. 2022. "Neural Correlates of Integration Processes during Dynamic Face Perception." *Scientific Reports* 12(January): 118.

Alp, Nihan, Andrey R. Nikolaev, Johan Wagemans, and Naoki Kogo. 2017. "EEG Frequency Tagging Dissociates between Neural Processing of Motion Synchrony and Human Quality of Multiple Point-Light Dancers." *Scientific Reports* 7(March): 44012.

Alp, Nihan, Peter Jes Kohler, Naoki Kogo, Johan Wagemans, and Anthony Matthew Norcia. 2018. "Measuring Integration Processes in Visual Symmetry with Frequency-Tagged EEG." *Scientific Reports* 8(May): 6969.

Anstis, Stuart. 2012. "The Furrow Illusion: Peripheral Motion Becomes Aligned with Stationary Contours." *Journal of Vision* 12(12).

Anstis, Stuart, and Juno Kim. 2011. "Local versus Global Perception of Ambiguous Motion Displays." *Journal of Vision* 11(March): 13–13.

Bair, Wyeth, and J. Anthony Movshon. 2004. "Adaptive Temporal Integration of Motion in Direction-Selective Neurons in Macaque Visual Cortex." *The Journal of Neuroscience* 24(August): 7305–7323.

Baker, C. L., and O. J. Braddick. 1985*a*. "Eccentricity-Dependent Scaling of the Limits for Short-Range Apparent Motion Perception." *Vision Research* 25(6): 803–812.

Baker, Curtis L, and Oliver J Braddick. 1985*b*. "Temporal Properties of the Short-Range Process in Apparent Motion." *Perception* 14(April): 181–192.

Battelli, L., P. Cavanagh, J. Intriligator, M. J. Tramo, M. A. Hénaff, F. Michèl, and J. J. Barton. 2001. "Unilateral Right Parietal Damage Leads to Bilateral Deficit for High-Level Motion." *Neuron* 32(December): 985–995.

Battelli, Lorella, Alvaro Pascual-Leone, and Patrick Cavanagh. 2007. "The 'When' Pathway of the Right Parietal Lobe." *Trends in Cognitive Sciences* 11(May): 204–210.

Boremanse, Adriano, Anthony M. Norcia, and Bruno Rossion. 2013. "An Objective Signature for Visual Binding of Face Parts in the Human Brain." *Journal of Vision* 13(September): 6–6.

Braddick, O. J., J. M. O'Brien, J. Wattam-Bell, J. Atkinson, T. Hartley, and R. Turner. 2001. "Brain Areas Sensitive to Coherent Visual Motion." *Perception* 30(1): 61–72.

Bradley, D. C., and R. A. Andersen. 1998. "Center-Surround Antagonism Based on Disparity in Primate Area MT." *The Journal of Neuroscience: The Official Journal of the Society for Neuroscience* 18(September): 7552–7565.

Burr, David, and Peter Thompson. 2011. "Motion Psychophysics: 1985-2010." *Vision Research* 51(July): 1431–1456.

Butler, Russell, Pierre-Michel Bernier, Gregory W. Mierzwinski, Maxime Descoteaux, Guillaume Gilbert, and Kevin Whittingstall. 2019. "Cortical Distance, Not Cancellation, Dominates Inter-Subject EEG Gamma Rhythm Amplitude." *NeuroImage* 192(May): 156–165.

Cavanagh, Patrick. 1992. "Attention-Based Motion Perception." *Science* 257(September): 1563–1565.

Clifford, Colin W. G., Damien J. Mannion, and J. Scott McDonald. 2009. "Radial Biases in the Processing of Motion and Motion-Defined Contours by Human Visual Cortex." *Journal of Neurophysiology* 102(November): 2974–2981.

Dahlem, A. Markus, and Jan Tusch. 2012. "Predicted Selective Increase of Cortical Magnification Due to Cortical Folding." *The Journal of Mathematical Neuroscience* 2(December): 14.

Daniel, P. M., and D. Whitteridge. 1961. "The Representation of the Visual Field on the Cerebral Cortex in Monkeys." *The Journal of Physiology* 159(December): 203–221.

Delorme, Arnaud, and Scott Makeig. 2004. "EEGLAB: An Open Source Toolbox for Analysis of Single-Trial EEG Dynamics Including Independent Component Analysis." *Journal of Neuroscience Methods* 134(March): 9–21.

Doerschner, Katja, Roland W. Fleming, Ozgur Yilmaz, Paul R. Schrater, Bruce Hartung, and Daniel Kersten. 2011. "Visual Motion and the Perception of Surface Material." *Current biology: CB* 21(December): 2010–2016.

Dow, B. M., A. Z. Snyder, R. G. Vautin, and R. Bauer. 1981. "Magnification Factor and Receptive Field Size in Foveal Striate Cortex of the Monkey." *Experimental Brain Research* 44(2): 213–228.

Emerson, R. C., J. R. Bergen, and E. H. Adelson. 1992. "Directionally Selective Complex Cells and the Computation of Motion Energy in Cat Visual Cortex." *Vision Research* 32(February): 203–218.

Er, Gorkem, Zahide Pamir, and Huseyin Boyaci. 2020. "Distinct Patterns of Surround Modulation in V1 and hMT+." *NeuroImage* 220(October): 117084.

Fahle, M. 1993. "Figure-Ground Discrimination from Temporal Information." *Proceedings of the Royal Society B: Biological Sciences* 254(1341): 199–203.

Faul, Franz, Edgar Erdfelder, Albert-Georg Lang, and Axel Buchner. 2007. "G*Power 3: A Flexible Statistical Power Analysis Program for the Social, Behavioral, and Biomedical Sciences." *Behavior Research Methods* 39(May): 175–191.

Gattass, Ricakdo, Aglai P. B. Sousa, and Marcello G. P. Rosa. 1987. "Visual Topography of V1 in the Cebus Monkey." *Journal of Comparative Neurology* 259(4): 529–548.

Georgeson, Mark A., and Michael G. Harris. 1990. "The Temporal Range of Motion Sensing and Motion Perception." *Vision Research* 30(January): 615–619.

Gordon, Noam, Jakob Hohwy, Matthew James Davidson, Jeroen J.A. van Boxtel, and Naotsugu Tsuchiya. 2019. "From Intermodulation Components to Visual Perception and Cognition-a Review." *NeuroImage* 199(October 2018): 480–494.

Horton, J. C., and W. F. Hoyt. 1991. "The Representation of the Visual Field in Human Striate Cortex. A Revision of the Classic Holmes Map." *Archives of Ophthalmology (Chicago, Ill.: 1960)* 109(June): 816–824.

Hubel, D. H., and T. N. Wiesel. 1959. "Receptive Fields of Single Neurones in the Cat's Striate Cortex." *The Journal of Physiology* 148(October): 574–591.

Hubel, D. H., and T. N. Wiesel. 1962. "Receptive Fields, Binocular Interaction and Functional Architecture in the Cat's Visual Cortex." *The Journal of Physiology* 160(1): 106–154.

Hubel, D. H., and T. N. Wiesel. 1968. "Receptive Fields and Functional Architecture of Monkey Striate Cortex." *The Journal of Physiology* 195(March): 215–243.

Huk, Alexander C., and David J. Heeger. 2002. "Pattern-Motion Responses in Human Visual Cortex." *Nature Neuroscience* 5(January): 72–75.

John, Ffion M., Nathan R. Bromham, J. Margaret Woodhouse, and T. Rowan Candy. 2004. "Spatial Vision Deficits in Infants and Children with Down Syndrome." *Investigative Ophthalmology & Visual Science* 45(May): 1566–1572.

Keil, Andreas, Edward M. Bernat, Michael X. Cohen, Mingzhou Ding, Monica Fabiani, Gabriele Gratton, Emily S. Kappenman, Eric Maris, Kyle E. Mathewson, Richard T. Ward, and Nathan Weisz. 2022. "Recommendations and Publication Guidelines for Studies Using Frequency Domain and Time-Frequency Domain Analyses of Neural Time Series." *Psychophysiology* 59(5): e14052.

Leopold, David A., Melanie Wilke, Alexander Maier, and Nikos K. Logothetis. 2002. "Stable Perception of Visually Ambiguous Patterns." *Nature Neuroscience* 5(June): 605–609.

Livingstone, M., and D. Hubel. 1988. "Segregation of Form, Color, Movement, and Depth: Anatomy, Physiology, and Perception." *Science (New York, N.Y.)* 240(May): 740–749.

Lorenceau, Jean, and David Alais. 2001. "Form Constraints in Motion Binding." *Nature Neuroscience* 4(July): 745–751.

Lu, Z. L., and G. Sperling. 2001. "Three-Systems Theory of Human Visual Motion Perception: Review and Update." *Journal of the Optical Society of America. A, Optics, Image Science, and Vision* 18(September): 2331–2370.

Maier, Alexander, Melanie Wilke, Nikos K. Logothetis, and David A. Leopold. 2003. "Perception of Temporally Interleaved Ambiguous Patterns." *Current biology: CB* 13(July): 1076–1085.

Maloney, Ryan T., Tamara L. Watson, and Colin W. G. Clifford. 2014. "Determinants of Motion Response Anisotropies in Human Early Visual Cortex: The Role of Configuration and Eccentricity." *NeuroImage* 100(October): 564–579.

Marr, D., and S. Ullman. 1981. "Directional Selectivity and Its Use in Early Visual Processing." *Proceedings of the Royal Society of London. Series B, Biological Sciences* 211(March): 151–180.

MATLAB. 2021. "MATLAB Version: 9.11.0 (R2021b)." The MathWorks Inc.

McDermott, J., Y. Weiss, and E. H. Adelson. 2001. "Beyond Junctions: Nonlocal Form Constraints on Motion Interpretation." *Perception* 30(8): 905–923.

Nishida, Shin'ya. 2011. "Advancement of Motion Psychophysics: Review 2001–2010." *Journal of Vision* 11(December): 11.

Nishida, Shin'Ya, Takahiro Kawabe, Masataka Sawayama, and Taiki Fukiage. 2018. "Motion Perception: From Detection to Interpretation." *Annual Review of Vision Science* 4(July): 501–523.

Norcia, Anthony M., L. Gregory Appelbaum, Justin M. Ales, Benolt R. Cottereaur, and Bruno Rossion. 2015. "The Steady State VEP in Research." *Journal of Vision* 15(6): 1–46.

Nozaradan, Sylvie, Isabelle Peretz, and André Mouraux. 2012. "Steady-State Evoked Potentials as an Index of Multisensory Temporal Binding." *NeuroImage* 60(March): 21–28.

Oostenveld, Robert, Pascal Fries, Eric Maris, and Jan-Mathijs Schoffelen. 2010. "FieldTrip: Open Source Software for Advanced Analysis of MEG, EEG, and Invasive Electrophysiological Data." *Computational Intelligence and Neuroscience* 2011(December): e156869.

Palmer, Chris R., Yuzhi Chen, and Eyal Seidemann. 2012. "Uniform Spatial Spread of Population Activity in Primate Parafoveal V1." *Journal of Neurophysiology* 107(April): 1857–1867.

Palomares, Melanie, Justin M. Ales, Alex R. Wade, Benoit R. Cottereau, and Anthony M. Norcia. 2012. "Distinct Effects of Attention on the Neural Responses to Form and Motion Processing: A SSVEP Source-Imaging Study." *Journal of Vision* 12(September): 15.

Pantle, Allan, and Lucinda Picciano. 1976. "A Multistable Movement Display: Evidence for Two Separate Motion Systems in Human Vision." *Science* 193(August): 500–502.

Park, Woon Ju, and Duje Tadin. 2018. "Motion Perception." In *Stevens' Handbook of Experimental Psychology and Cognitive Neuroscience*. John Wiley & Sons, Ltd pp. 1–73.

Peirce, Jonathan, Jeremy R. Gray, Sol Simpson, Michael MacAskill, Richard Höchenberger, Hiroyuki Sogo, Erik Kastman, and Jonas Kristoffer Lindeløv. 2019. "PsychoPy2: Experiments in Behavior Made Easy." *Behavior Research Methods* 51(February): 195–203.

Pitchaimuthu, Kabilan, Giulia Dormal, Suddha Sourav, Idris Shareef, Siddhart S. Rajendran, José Pablo Ossandón, Ramesh Kekunnaya, and Brigitte Röder. 2021. "Steady State Evoked Potentials Indicate Changes in Nonlinear Neural Mechanisms of Vision in Sight Recovery Individuals." *Cortex; a Journal Devoted to the Study of the Nervous System and Behavior* 144(November): 15–28.

Raemaekers, Mathijs, Martin J.M. Lankheet, Sanne Moorman, Zoe Kourtzi, and Richard J.A. van Wezel. 2009. "Directional Anisotropy of Motion Responses in Retinotopic Cortex." *Human Brain Mapping* 30(May): 3970–3980.

Regan, D. 1977. "Steady-State Evoked Potentials." *Journal of the Optical Society of America* 67(November): 1475–1489.

Reichardt, W. 1961. Autocorrelation, a Principle for Evaluation of Sensory Information by the Central Nervous System. In *Symposium on Principles of Sensory Communication 1959*. MIT Press pp. 303–317.

Retter, Talia L., and Bruno Rossion. 2016. "Uncovering the Neural Magnitude and Spatio-Temporal Dynamics of Natural Image Categorization in a Fast Visual Stream." *Neuropsychologia* 91(October): 9–28.

Retter, Talia L., Bruno Rossion, and Christine Schiltz. 2021. "Harmonic Amplitude Summation for Frequency-tagging Analysis." *Journal of Cognitive Neuroscience* 33(October): 2372–2393.

Rice, Justin K., Christopher Rorden, Jessica S. Little, and Lucas C. Parra. 2013. "Subject Position Affects EEG Magnitudes." *NeuroImage* 64(January): 476–484.

Rossion, Bruno, Katrien Torfs, Corentin Jacques, and Joan Liu-Shuang. 2015. "Fast Periodic Presentation of Natural Images Reveals a Robust Face-Selective Electrophysiological Response in the Human Brain." *Journal of Vision* 15(January): 18.

Schaul, Neil. 1998. "The Fundamental Neural Mechanisms of Electroencephalography." *Electroencephalography and Clinical Neurophysiology* 106(February): 101–107.

Schellekens, Wouter, Richard J. A. Van Wezel, Natalia Petridou, Nick F. Ramsey, and Mathijs Raemaekers. 2013. "Integration of Motion Responses Underlying Directional Motion Anisotropy in Human Early Visual Cortical Areas." *PLoS ONE* 8(June): e67468.

Scholl, B. J., and P. D. Tremoulet. 2000. "Perceptual Causality and Animacy." *Trends in Cognitive Sciences* 4(August): 299–309.

Schwartz, Eric L. 1980. "Computational Anatomy and Functional Architecture of Striate Cortex: A Spatial Mapping Approach to Perceptual Coding." *Vision Research* 20(January): 645–669.

Seiffert, Adriane E, and Patrick Cavanagh. 1998. "Position Displacement, Not Velocity, Is the Cue to Motion Detection of Second-Order Stimuli." *Vision Research* 38(November): 3569–3582.

Seiffert, Adriane E, and Patrick Cavanagh. 1999. "Position-Based Motion Perception for Color and Texture Stimuli: Effects of Contrast and Speed." *Vision Research* 39(December): 4172–4185.

Silva, Maria Fatima, Jan W. Brascamp, Sónia Ferreira, Miguel Castelo-Branco, Serge O. Dumoulin, and Ben M. Harvey. 2018. "Radial Asymmetries in Population Receptive Field Size and Cortical Magnification Factor in Early Visual Cortex." *NeuroImage* 167(February): 41–52.

Tadin, Duje, Joseph S. Lappin, Lee A. Gilroy, and Randolph Blake. 2003. "Perceptual Consequences of Centre–Surround Antagonism in Visual Motion Processing." *Nature* 424(July): 312–315.

Talbot, S. A., and W. H. Marshall. 1941. "Physiological Studies on Neural Mechanisms of Visual Localization and Discrimination*." *American Journal of Ophthalmology* 24(November): 1255–1264.

The jamovi project. 2022. "Jamovi.".

Tootell, R. B., E. Switkes, M. S. Silverman, and S. L. Hamilton. 1988. "Functional Anatomy of Macaque Striate Cortex. II. Retinotopic Organization." *Journal of Neuroscience* 8(May): 1531–1568.

Trimble, Charles R. 1968. "What Is Signal Averaging." *Hewlett-Packard Journal* 19(8): 2–7.

Van Essen, D. C., W. T. Newsome, and J. H. Maunsell. 1984. "The Visual Field Representation in Striate Cortex of the Macaque Monkey: Asymmetries, Anisotropies, and Individual Variability." *Vision Research* 24(5): 429–448.

Varlet, Manuel, Sylvie Nozaradan, Richard C. Schmidt, and Peter E. Keller. 2023. "Neural Tracking of Visual Periodic Motion." *European Journal of Neuroscience* n/a(February): 1–17.

Vergeer, Mark, Naoki Kogo, Andrey R. Nikolaev, Nihan Alp, Veerle Loozen, Brenda Schraepen, and Johan Wagemans. 2018. "EEG Frequency Tagging Reveals Higher Order Intermodulation Components as Neural Markers of Learned Holistic Shape Representations." *Vision Research* 152(November): 91–100.

Verstraten, F. A., P. Cavanagh, and A. T. Labianca. 2000. "Limits of Attentive Tracking Reveal Temporal Properties of Attention." *Vision Research* 40(26): 3651–3664.

Wallach, H. 1935. "Über Visuell Wahrgenommene Bewegungsrichtung. [On the Visually Perceived Direction of Movement.]." *Psychologische Forschung* 20: 325–380.

Wandell, Brian A., Serge O. Dumoulin, and Alyssa A. Brewer. 2007. "Visual Field Maps in Human Cortex." *Neuron* 56(October): 366–383.

Watson, A. B., and A. J. Ahumada. 1985. "Model of Human Visual-Motion Sensing." *Journal of the Optical Society of America. A, Optics and Image Science* 2(February): 322–341.

Wolfe, Jeremy M., Keith R. Kluender, and Dennis M. Levi. 2020. *Sensation & Perception*. Sixth edition ed. New York: Sinauer Associates: Oxford University Press.

Zharikova, Aleksandra, Sergei Gepshtein, and Cees van Leeuwen. 2017. "Paradoxical Perception of Object Identity in Visual Motion." *Vision Research* 136(July): 1–14.